Arrested development: Erosional equilibrium in the southern Sierra Nevada, California, maintained by feedbacks between channel incision and hillslope sediment production

Russell P. Callahan[1,2,†], Ken L. Ferrier[3,4], Jean Dixon[5], Anthony Dosseto[6], W. Jesse Hahm[7], Barbara S. Jessup[1], Scott N. Miller[2,8], Carolyn T. Hunsaker[9], Dale W. Johnson[10], Leonard S. Sklar[11], and Clifford S. Riebe[1,2]

[1]*Department of Geology and Geophysics, University of Wyoming, Laramie, Wyoming 82071, USA*
[2]*Wyoming Center for Environmental Hydrology and Geophysics, University of Wyoming, Laramie, Wyoming 82071, USA*
[3]*School of Earth and Atmospheric Sciences, Georgia Institute of Technology, Atlanta Georgia 30332, USA*
[4]*Department of Geoscience, University of Wisconsin, Madison, Wisconsin 53706, USA*
[5]*Department of Earth Sciences, Montana State University, Bozeman, Montana 59717, USA*
[6]*Wollongong Isotope Geochronology Laboratory, School of Earth and Environmental Sciences, University of Wollongong, Wollongong, NSW 2522, Australia*
[7]*Department of Earth and Planetary Science, University of California, Berkeley, California 94720, USA*
[8]*Department of Ecosystem Science and Management, University of Wyoming, Laramie, Wyoming 82071, USA*
[9]*Pacific Southwest Research Station, Forest Service, U.S. Department of Agriculture, Fresno, California 93710, USA*
[10]*Department of Natural Resources and Environmental Sciences, University of Nevada, Reno, Nevada 89557, USA*
[11]*Department of Geography, Planning & Environment, Concordia University, Montreal, Quebec H3G 1M8, Canada*

ABSTRACT

Tributary creeks of the southern Sierra Nevada have pronounced knickpoints that separate the landscape into an alternating sequence of gently sloped treads and steeply sloped risers. These knickpoints and the surrounding "stepped topography" suggest that the landscape is still responding to Pleistocene changes in base level on mainstem rivers. We tested this hypothesis using cosmogenic nuclides and uranium isotopes measured in stream sediment from widely distributed locations. Catchment-scale erosion rates from the cosmogenic nuclides suggest that the treads are relict surfaces that have adjusted to a previous base level. Nevertheless, erosion rates of relict interfluves are similar to canyon incision rates, implying that relief is unchanging in the lower Kings and San Joaquin Rivers. In addition, our results suggest that much of the southern Sierra Nevada is in a state of arrested development: the landscape is not fully adjusted to—and moreover is not responding to— changes in base-level lowering in the canyons. We propose that this can be explained by a paucity of coarse sediment sup-ply, which fails to provide sufficient tools for bedrock channel incision at knickpoints. We hypothesize that the lack of coarse sediment in channels is driven by intense weathering of the local granitic bedrock, which reduces the size of sediment supplied from hillslopes to the channels. Our analysis highlights a feedback in which sediment size reduction due to weathering on hillslopes and transport in channels is both a key response to and control of bedrock channel incision and landscape adjustment to base-level change.

INTRODUCTION

Landscape adjustment to base-level change is controlled by complex feedbacks between weathering, climate, tectonics, and erosion (e.g., Whipple and Tucker, 1999; Whipple, 2004; Cowie et al., 2008; DiBiase et al., 2018). Tectonically driven base-level lowering sets the pace of channel incision, which influences hillslope erosion rates (Granger et al., 1996; Riebe et al., 2000; Wobus et al., 2006; Whittaker et al., 2007; DiBiase et al., 2012). Hillslope erosion, in turn, sets the rate of sediment supply to rivers and thus provides the tools needed for bedrock channel incision, creating a feedback between hillslope sediment production and channel incision (Egholm et al., 2013; Sklar et al., 2017). This feedback is modulated by the sizes of hillslope-sourced sediment, which can influence channel incision rate (Sklar and Dietrich, 1998, 2001, 2004), thereby indirectly affecting hillslope erosion rate, the duration of weathering (Yoo and Mudd, 2008), and thus also the sizes of sediment produced on slopes (Attal et al., 2015; Riebe et al., 2015). Sediment size also depends on weathering intensity (e.g., Marshall and Sklar, 2012; Riebe et al., 2015; Sklar et al., 2017), which is affected by climate (Riebe et al., 2004; Dixon et al., 2009a; Ferrier et al., 2016), and climate in turn has well-known feedbacks with silicate weathering, a long-term sink for atmospheric CO_2 (Walker et al., 1981; Berner et al., 1983; Maher and Chamberlain, 2014). Thus, by influencing bedrock channel incision, tectonically driven base-level lowering can influence rates of hillslope erosion, silicate weathering, and CO_2 drawdown, thereby modulating global climate over millions of years (Raymo et al., 1988; Riebe et al., 2004; Ferrier et al., 2016). In addition, hillslopes and channels are coupled by the climatically mediated production and delivery of sediment from hillslopes to channels through their influence on rates of channel incision and landscape response to tectonic changes in base level (Sklar et al., 2017).

Although landscape response to tectonic forcing depends on the ways in which channels and hillslopes interact (e.g., Pelletier, 2007; Egholm et al., 2013; Shobe et al., 2016), the

†rcallaha@uwyo.edu

feedbacks between them remain poorly understood because rates of hillslope erosion and channel incision have only been measured together in a few locations (e.g., Cyr and Granger, 2008; Cyr et al., 2010; Willenbring et al., 2013b; Brocard et al., 2016). Here, we explore landscape response to changes in incision rates in the Sierra Nevada, California (Fig. 1), which has been a nexus of research on mountain landscape evolution for more than a century (Lindgren, 1911; Hake, 1928; Panzer, 1933; Matthes, 1960; Wahrhaftig, 1965; Huber, 1981; Unruh, 1991; Small and Anderson, 1995; Stock et al., 2004; Cassel et al., 2009; Gabet, 2014). Previous researchers have produced vast sets of geologic, geomorphic, geodetic, and isotopic data (House et al., 1997; Clark et al., 2005; Mulch et al., 2006; Cassel et al., 2009; McPhillips and Brandon, 2012; Hurst et al., 2012; Gabet, 2014; Hammond et al., 2016) that have helped to constrain uplift, erosion, weathering, and river incision (House et al., 1998; Riebe et al., 2000, 2001b, 2015; Granger et al., 2001; Waka-

bayashi and Sawyer, 2001; Stock et al., 2005; Dixon et al., 2009a) across much of the mountain range and over time scales ranging from a few years to tens of millions of years (Saleeby et al., 2003; Stock et al., 2004; Hammond et al., 2016; Hunsaker and Neary, 2012; Wakabayashi, 2013; Sousa et al., 2016; Wheeler et al., 2016; Krugh and Foreshee, 2018). Most importantly for our study, many studies in the region have used cosmogenic nuclides to quantify both physical and chemical erosion rates (Granger et al., 1996; Small et al., 1997; Riebe et al., 2000, 2001a, 2001b, 2015; Granger et al., 2001; Stock et al., 2004, 2005, 2006; Dixon et al., 2009a, 2009b; Hurst et al., 2012, 2013; Hahm et al., 2014; Attal et al., 2015). In particular, our study area features numerous cosmogenic nuclide–based estimates of interfluve erosion rates (Stock et al., 2004), soil production rates (Dixon et al., 2009a, 2009b), chemical erosion rates of saprolite and soil (Dixon et al., 2009a, 2009b; Riebe and Granger, 2013), catchment-averaged estimates of total (i.e., chemical plus physical)

erosion rates (Hahm et al., 2014), and river incision rates (Stock et al., 2004, 2005). Together, these data inform a quantitative understanding of landscape evolution that makes the region well suited for studying connections between tectonics, channel incision, and hillslope sediment production.

Our study area lies on the western slope of the southern Sierra Nevada, which is widely thought to be out of topographic equilibrium (Clark et al., 2005), with hillslopes and channels that are still adjusting to regional changes in climate and tectonics (Wakabayashi and Sawyer, 2001; Stock et al., 2004; McPhillips and Brandon, 2010; Gabet, 2014). We focused on the area between the Kings and San Joaquin Rivers (Fig. 1A), where previous work nearby shows that river incision rates declined by a factor of ~13 over the Pleistocene (Stock et al., 2004, 2005). At a coarse scale, the region is characterized by narrow, deeply incised canyons (Fig. 1B) separated by broad, gently sloped upland hillslopes (referred to here as "interfluves";
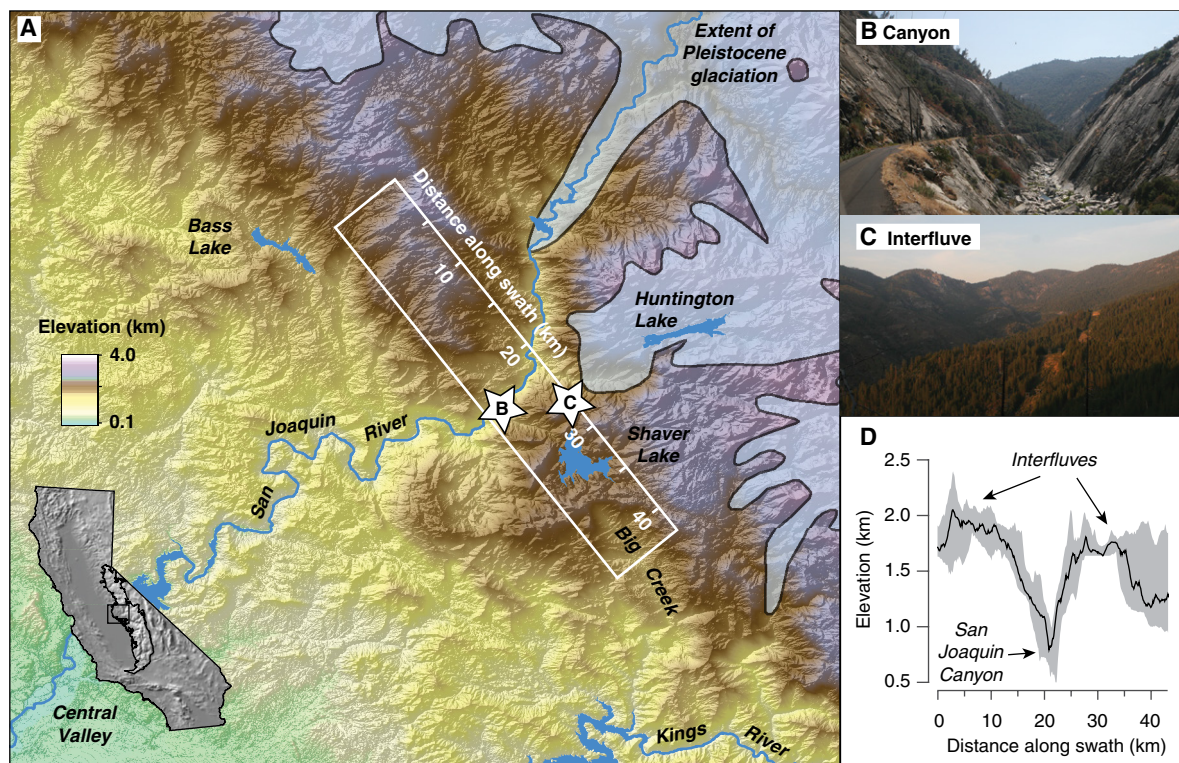
Figure 1. Interfluves and canyons of the southern Sierra Nevada. (A) Map of the western slope of the Sierra Nevada showing range-parallel swath (white box) spanning interfluves and canyon of the San Joaquin River, with shaded relief map of California, USA (inset), showing map area (box) within the Sierra Nevada Batholith (black outline). Opaque area at upper right marks extent of Pleistocene glaciation (after Gillespie and Zehfuss, 2004). (B–C) Contrasts in terrain, where stars in A mark canyon (B) and upland interfluve (C). Typical relief in B is >1000 m while relief in C is <500 m. (D) Distribution of elevation along the swath in A showing the characteristic deep canyon and broad interfluve topography. Line marks median, and gray band spans the inner 95% of elevations along the swath.

Fig. 1C), consistent with a landscape in which changes in base-level lowering have not fully propagated through the channel network (Stock et al., 2004).

At a finer scale (Fig. 2), streams and hillslopes are organized into series of steep risers and gentle treads resembling an irregular staircase (Wahrhaftig, 1965), suggesting that base-level changes are still propagating upstream as the series of knickpoints visible as channel profile convexities at the transitions between risers and treads (Figs. 2B and 2D). This prominent "stepped topography" (Fig. 2) is specific to the southern part of the range and is limited to the Sierra Nevada Batholith, implying a connection to granitic bedrock (Wahrhaftig, 1965); alternating risers and treads are absent in the northern Sierra Nevada, where metamorphic and volcanic bedrock is more common (e.g., Wakabayashi and Sawyer, 2001). Despite the apparent connection to lithology, the origin of the stepped topography remains enigmatic. Early work proposed that some of the larger steps in the range might be due to normal faulting along the western Sierra fault system (Hake, 1928). An alternative explanation, proposed by Panzer (1933), is that the topography of the western Sierra Nevada reflects erosional responses to pulses of uplift that are migrating from low to high elevations in the range, similar to the Piedmonttreppen hypothesis of Penck (1924). Still another possibility, first proposed by Wahrhaftig (1965), is that the steps originated from feedbacks involving preferential exposure of bare, erosion-resistant granitic bedrock on steep slopes.

New and existing cosmogenic nuclide data from the region allowed us to test several of the hypotheses about the origin and evolution of the region's characteristic stepped topography (Fig. 2). For example, by comparing cosmogenic nuclide–based erosion rates of risers and treads in the region, we can determine whether the steps are migrating upstream through the drainage network in response to changes in base-level lowering in the canyons, thus testing the Piedmonttreppen hypothesis of Penck (1924). In this study, we define a "step" to be a single tread-riser sequence. If the cosmogenic nuclides show that steep risers are eroding faster than the gently sloping treads, as might be expected from some published relationships between erosion rate and hillslope gradient (Granger et al., 1996; Riebe et al., 2000, 2015; DiBiase et al., 2012; Willenbring et al., 2013a; Larsen et al., 2014), then the risers should be eroding headward through the treads, carrying any signals of base-level lowering toward the interfluves.

An alternate hypothesis, which we also tested, is that the stepped topography is laterally stable because the gentle treads and steep risers are eroding downward at the same rate (Wahrhaftig, 1965). If true, then the steps should remain laterally in place as they lower, such that any headward-migrating signals of base-level lowering have stagnated. A special case of this hypothesis, first proposed by Wahrhaftig (1965), is that steps are eroding in place without headward migration due to a dominance of transport-limited erosion on gentle soil-mantled treads and weathering-limited erosion on steep bedrock risers (Gilbert, 1877; Wahrhaftig, 1965; Carson and Kirkby, 1972; Granger et al., 2001; Riebe et al., 2017). Our analysis compares erosion rates between bedrock and soil-mantled examples of both steep risers and gently sloped treads, allowing us to test Wahrhaftig's hypothesis about weathering and transport limitations on erosion. We also used uranium isotope ratios in sediment to explore weathering mechanisms on the risers and treads (Chabaux et al., 2006; Dosseto et al., 2008a, 2014).

In addition to exploring the origin and evolution of the stepped topography, our analysis also addresses several other hypotheses about landscape evolution in the region. For example, it has been proposed that relief is growing between the broad upland interfluves and deep narrow canyons (McPhillips and Brandon, 2010), and that the interfluves (Fig. 1C) are relict features (Stock et al., 2005), i.e., remnants of a slowly eroding landscape that has not yet been influenced by Pleistocene base-level lowering (Riebe et al., 2000; Wakabayashi and Sawyer, 2001; Stock et al., 2004, 2005; Wakabayashi, 2013). We tested this hypothesis using new and existing measurements of interfluve erosion rates from outcrops (Small et al., 1997; Stock et al 2005) and new catchment-averaged total interfluve erosion rates from cosmogenic nuclides in stream sediment (Hahm et al., 2014). Our sampling of "nested" catchments (of varying size and distance from the outlet) allowed us to detect spatial variations in erosion rates and thus quantify landscape response to changes in base-level lowering over time (e.g., Willenbring et al., 2013b). Thus, our results help resolve lingering debate about whether relief is growing, declining, or remaining roughly constant in the region (Stock et al., 2005; McPhillips and Brandon, 2010).

Our data indicate that the erosion rates of the treads and risers are roughly the same on average, despite the marked differences in hillslope gradient between them. This implies that the risers are laterally stable; i.e., they do not migrate headward very quickly as the landscape erodes downward. However, our results also suggest that weathering and transport limitations on erosion cannot explain the lateral stability of the steps, contrary to Wahrhaftig's hypothesis.

Given that the steps generally coincide with knickpoints in the channel network (Fig. 2), the lateral stability of the stepped topography implies that the knickpoints are likewise not migrating headward through the system. Nevertheless, we suggest that the staircase of risers and treads that dominates elevation gain on the western slope of the range reflects a landscape response to recent pulses of uplift that may have been driven by glacial-interglacial changes in climate during the Pleistocene. Together, our observations suggest that much of the southern Sierra Nevada landscape is in a state of arrested development: It has not fully adjusted to—and moreover does not appear to be responding to—the observed order-of-magnitude changes in incision rates over the last 2.7 m.y. To explain this, we propose a new hypothesis: The arrested development of the landscape is dictated by a paucity of coarse sediment supply from hillslopes to channels, which in turn is a consequence of intense weathering of the region's granitic bedrock. Long residence time during fluvial sediment transport across gentle treads may also contribute to particle weathering and thus grain-size reduction. The resulting lack of coarse tools for channel incision into bedrock inhibits headward migration of bedrock knickpoints at the transitions between risers and treads. Thus, our analysis highlights a plausible feedback in which weathering and erosion of hillslopes influence landscape response to base-level changes through their influence on bedrock river incision, which in turn influences the production and erosion of hillslope sediment.

STUDY AREA

Our analyses focused on mostly unglaciated terrain on the western slope of the Sierra Nevada, in Fresno and Madera Counties, California, USA (Fig. 1). The study area is underlain by the Sierra Nevada Batholith, a province of mostly Mesozoic plutons ranging in composition from gabbro to leucogranite, with granite, granodiorite, and tonalite being most common (e.g., Bateman, 1992; Lackey et al., 2012). Our study catchments range in average elevation from 144 to 2959 m within a zone dominated by stepped topography (Wahrhaftig, 1965; Jessup et al., 2011); it has been argued that the alternating risers and treads account for much of the first ~2000 m of elevation gain within the range (Wahrhaftig, 1965).

The large elevation gradient spanned by our study catchments drives marked contrasts in climate and vegetation. Mean annual precipitation varies from 43 to 134 cm yr^{-1} (PRISM, 2017), and mean annual temperature varies from 5 °C to 17 °C (PRISM, 2017). Vegetation covaries with
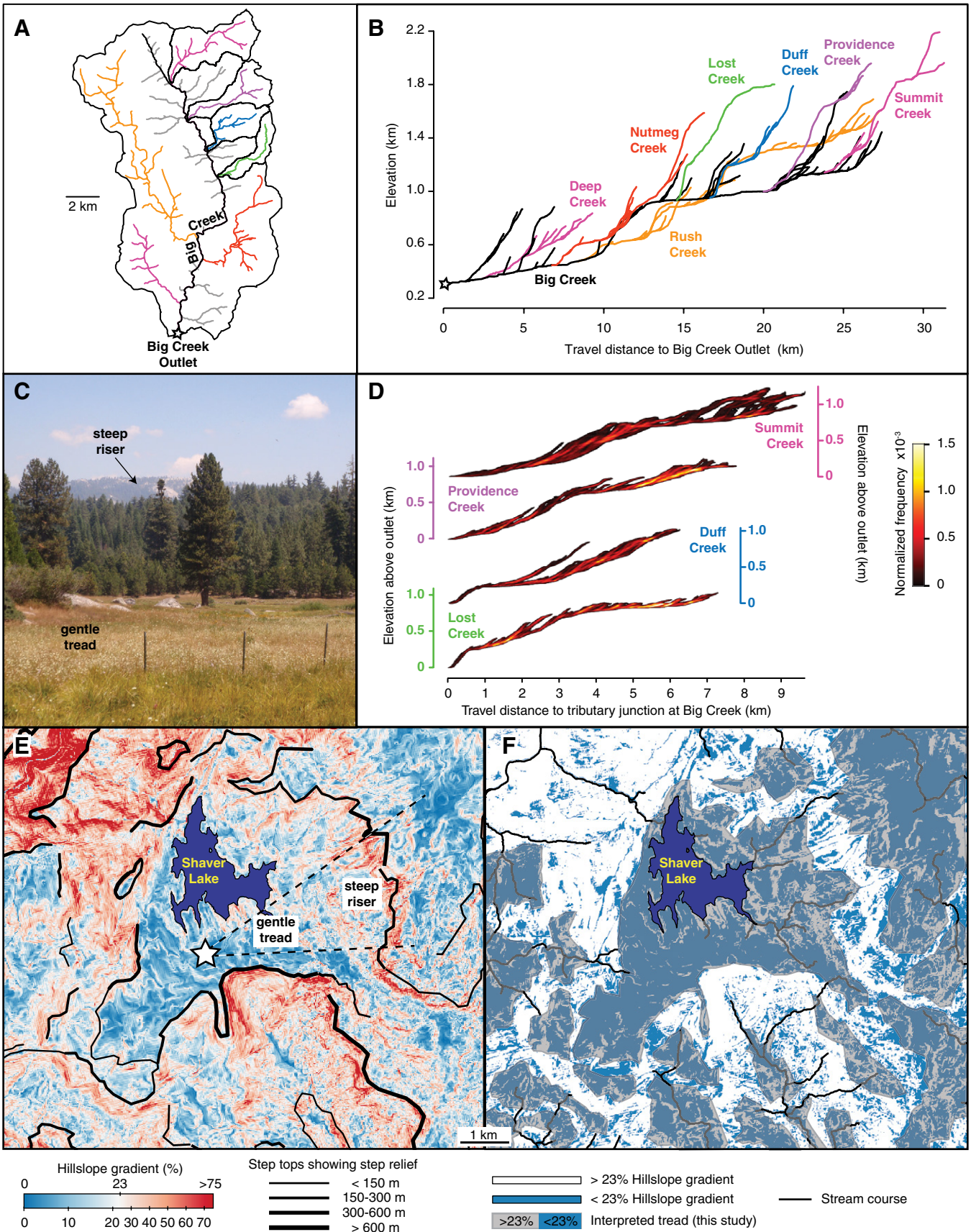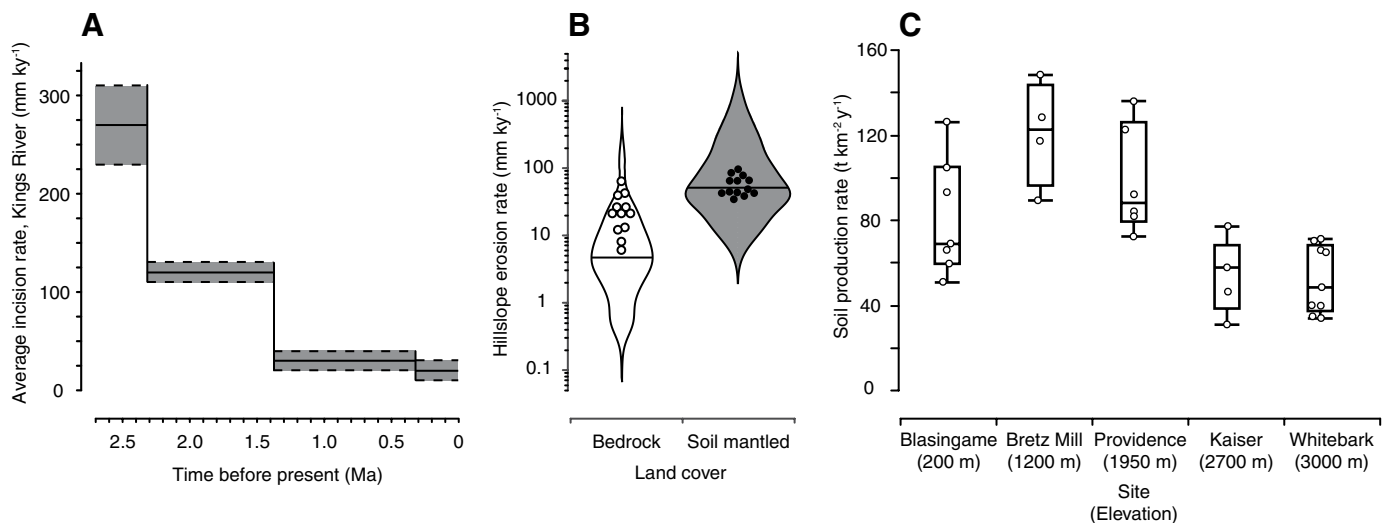
Figure 2.

Figure 2. Stepped topography of the southern Sierra Nevada. (A) Map of Big Creek with streams colored by tributary. (B) Longitudinal profiles of Big Creek tributaries, showing pronounced convexities that coincide with step tops (at the upper ends of risers). (C) Image of a gently sloping soil-mantled tread (foreground) and a steeply sloping bedrock riser (background). (D) Longitudinal landscape profiles (after Sklar et al., 2016) for several catchments that drain to Big Creek. Color scale shows normalized frequency of points on the landscape that have the same elevation and travel distance from outlet at Big Creek. Marked steps in each profile suggest that the hillslopes are organized into a series of perched low-relief surfaces separated by steep hillslopes at knickpoints. (E) Hillslope gradient map of Shaver Lake area, with step fronts (black lines) digitized from Wahrhaftig's (1965) map. Line thickness denotes relief between step top and the tread immediately below it. Star marks location of photo, and dashed lines span approximate field of view in C. (F) Mapped step tops generally correspond to sharp contrasts in hillslope gradient, providing a basis for mapping the extent of individual treads, defined by roughly contiguous areas of <23% hillslope gradient (gray shaded areas). The geometry of treads and risers allowed us to select study catchments that exclusively drain risers and treads as distinct landscape elements.

these climatic variations, ranging from sparsely canopied oak-savannah woodlands at low elevations to densely canopied mixed-conifer forests dominated by white fir at high elevations. The altitudinal contrast in vegetation is reflected in variations in evapotranspiration rate (Goulden and Bales, 2014), a measure of ecosystem productivity; tower eddy-covariance data indicate that evapotranspiration peaks at middle elevations, which appear to be less affected by water limitations that curtail growth during summer at lower elevations and a shorter growing season at higher elevations due to lower temperatures during winter (Goulden et al., 2012). Although the vast majority of our study catchments were not covered by ice during the Pleistocene (Gillespie and Zehfuss, 2004), many likely experienced periglacial conditions, with differing vegetation, erosion, and sediment production processes (e.g., Woolfenden, 2003; Madoff and Putkonen, 2016; Marshall et al., 2017).

The altitudinal differences in climate and vegetation are reflected in soil development, which has been intensively studied in the region for decades (e.g., Jenny et al., 1949; Arkley, 1981; Dahlgren et al., 1997; Dixon et al., 2009a, 2009b; Graham et al., 2010). A key finding from previous work is that soil production rates, soil thickness, clay content, and secondary iron-oxide concentrations exhibit humped altitudinal relationships with peaks at middle elevations that roughly coincide with the modern rain-snow transition (Fig. 3C; Dahlgren et al., 1997; Dixon et al., 2009a, 2009b)—defined as the elevation above which snow dominates over rain as a precipitation source (Bales et al., 2011). Meanwhile, subsoil images from seismic refraction surveys reveal thick, highly porous saprolite (Holbrook et al., 2014) that generally increases in thickness with elevation across the first 2000 m of relief in the range (Klos et al., 2018). Water stored in saprolite and weathered

Figure 3. Results from previous cosmogenic nuclide studies. (A) Cosmogenic nuclide burial dating of cave sediment perched at different elevations above the modern Kings River reveals a marked decrease in incision rates over time since the early Pleistocene (after Stock et al., 2005). Gray band spans ±1 standard error of estimated incision rate. (B) Distribution of total erosion rates (note log scale) in bedrock (open) and soil-mantled (shaded) granitic terrain of the southern Sierra Nevada (circles; after Hahm et al., 2014) and from a global compilation of granitic terrain (violin plots; based on data compiled by Portenga and Bierman, 2011), showing that bedrock areas tend to erode slower than soil-mantled areas in granitic landscapes. Width of each "violin" shows relative frequency normalized to number of samples in global compilation (*n* = 250 for bedrock and *n* = 416 for soil-mantled categories) at widest point of violin. Horizontal bar shows median of the global compilation. (C) Soil production rates measured using cosmogenic nuclides from five sites across an elevation gradient within our study area (after Dixon et al., 2009a). The relationship between soil production and elevation suggests a humped trend, where soil is produced faster at midelevation sites, possibly due to climatic differences.

rock is evidently crucial to sustaining above-ground biomass during the region's dry summers and prolonged droughts (Arkley 1981; Graham et al., 2010; Bales et al., 2011; Klos et al., 2018). It is therefore possible that the altitudinal increase in saprolite thickness partly explains the observed increase in ecosystem productivity from low to intermediate elevations (Klos et al., 2018). Forests at middle elevations are also supported by nutrients carried in dust, according to recent estimates of dust fluxes (Aciego et al., 2017) and dust-derived nutrient incorporation into vegetation (Arvin et al., 2017).

Several cosmogenic nuclide data sets contributed to the analyses presented here. River incision rates, derived from burial dating of cave sediment (Stock et al., 2004, 2005), declined by a factor of ~13, from 270 mm k.y.$^{-1}$ to 20 mm k.y.$^{-1}$, over the last 2.7 m.y. on the Kings River (Fig. 3A) after a prolonged, pre-Pleistocene period of stable base level (Stock et al., 2004, 2005). In contrast, erosion rates, derived from exposure dating of outcrops, indicate that bedrock interfluves are eroding slowly compared to the fast canyon incision of the early Pleistocene (Small et al., 1997; Stock et al., 2004, 2005). Cosmogenic nuclide–based analyses of soil production rates (Fig. 3C) have revealed the critical importance of saprolite weathering in soil production and erosion in the region (Dixon, 2008; Dixon et al., 2009a, 2009b); chemical depletion measurements imply a trade-off between saprolite and soil weathering, wherein little soil weathering occurs over highly depleted saprolite, and substantial soil weathering occurs over weakly depleted saprolite (Dixon et al., 2009a). In addition, a study of land cover, lithology, and cosmogenic nuclide–based estimates of total erosion rates across middle elevations in the region showed that sparsely vegetated, bedrock areas erode slower than densely canopied, soil-mantled areas (Fig. 3B); the variations in bedrock bulk geochemistry across the sites, though small, can explain much of the variation in forest cover and therefore erosion rates (Hahm et al., 2014). Here, we expand on the observations in Figure 3 and explore patterns in erosion rates and the distribution of the region's stepped topography to evaluate landscape response to changes in river incision rates.

METHODS

Experimental Design

Comparisons of catchment-averaged erosion rates to river incision rates reveal whether relief is currently growing, declining, or remaining roughly constant between rivers and surrounding hillslopes. It also helps to reveal the degree to which the landscape has adjusted to changes in river incision over time (e.g., Willenbring et al., 2013b). Because our compilation contains several sets of nested catchments (e.g., Fig. 4A), we were able to quantify variations in hillslope erosion rates as a function of distance from a downstream base-level reference point—in this case, the main stem of either the Kings River or San Joaquin River. If erosion rates vary markedly with distance from base level, then the landscape is not in equilibrium; i.e., the tributaries and hillslopes have not fully adjusted to changes in base level. In the case of the Sierra Nevada, which can be broadly divided into deep canyons separated by broad interfluves (Fig. 1D), an increase in erosion rates with distance from the canyons implies that the broad interfluves (Fig. 1C) are eroding faster than canyons, and that relief—on a broad scale—is declining. Conversely, a decrease in erosion rates with distance from the canyons implies that canyon-to-interfluve relief is increasing.

To evaluate the proposed hypotheses about the evolution of stepped topography in Figures 4D and 4E, we identified two sets of catchments: one that drains only risers and another that drains only treads (e.g., Fig. 4C). We further classified these treads and risers based on dominance of bedrock or soil as a land cover type. Thus, we were able to directly compare erosion rates across the four combinations of land-cover and landscape categories that are relevant to testing Wahrhaftig's (1965) hypothesis: bedrock treads, soil-mantled treads, bedrock risers, and soil-mantled risers. According to Wahrhaftig (1965), bedrock risers should be eroding at the same rate as soil-mantled treads. However, Wahrhaftig's hypothesis—that landscape evolution on the western slope of the southern Sierra Nevada is governed by weathering limitations on risers and transport limitations on treads—relies on the assumption that the most common combination of landscape categories in the stepped topography is bedrock risers in front of soil-mantled treads. In particular, Wahrhaftig's hypothesis requires that bedrock dominates at transitions between the upper edges of risers and the next higher treads. If bedrock is abundant and if erosion is weathering-limited at a transition, it can act as a static base level for the adjacent soil-mantled tread, which can then reduce its slope further by erosion to the elevation of the transition. To determine whether the required land-cover combination is common enough to support Wahrhaftig's hypothesis, we quantified the fractional coverage of vegetated soil-mantled and bedrock areas on a random sample of risers, transitions, and treads

from the southern Sierra Nevada (as described later herein).

Cosmogenic Nuclides

For a comprehensive perspective on hillslope erosion rates in the region, we combined new measurements of catchment-averaged erosion rates with previously published catchment-averaged total erosion rates (Hahm et al., 2014) and point erosion rate measurements from interfluves (Stock et al., 2004, 2005; Hahm et al., 2014), all based on cosmogenic nuclide measurements (e.g., Dixon and Riebe, 2014; Granger and Riebe, 2014). Our compilation also includes previously published erosion rates from bedrock outcrops on interfluves (Stock et al., 2004, 2005; Hahm et al., 2014) and soil production rates from within several of the study catchments (Dixon et al., 2009a, 2009b), providing additional perspective on sediment production in the region.

The outcrop samples were collected from exfoliation slabs (Stock et al., 2005) or from bare rock surfaces using a gasoline-powered Pomeroy™ rock drill with a 4-in.-diameter (~10-cm-diameter) bit (Hahm et al., 2014). To obtain representative samples for the catchment-averaged erosion rates, we collected bed sediment from multiple locations along the channel. The sediment typically spanned a narrow range of sizes, including mostly sand and fine gravel. Thus, our analyses should be largely free of erosion rate biases expected in catchments with wider sediment size distributions (Lukens et al., 2016).

In total, we sampled sediment from streams at 58 locations within the Kings and San Joaquin River watersheds. We also considered data from nine samples of bedrock, including four previously reported values that we report here without modification, i.e., as they were presented in previous work (Stock et al., 2004, 2005). Thirty-five of the total 67 samples were prepared using University of Wyoming facilities. Twenty-eight samples were prepared at Dartmouth College facilities using procedures that differed, as described below, from protocols used at Wyoming (Dixon, 2008). At five of the streams in our study, we collected sediment on separate occasions (2004 and 2009), prepared the samples in different laboratories (Dartmouth and University of Wyoming), and analyzed them for cosmogenic nuclides at different accelerator mass spectrometry (AMS) facilities: the Center for Accelerator Mass Spectrometry (CAMS) and the Purdue Rare Isotope Measurement (PRIME) Laboratory. This allowed us to evaluate the consistency of measured [10]Be concentrations between the different approaches used by our team. It also helped to determine
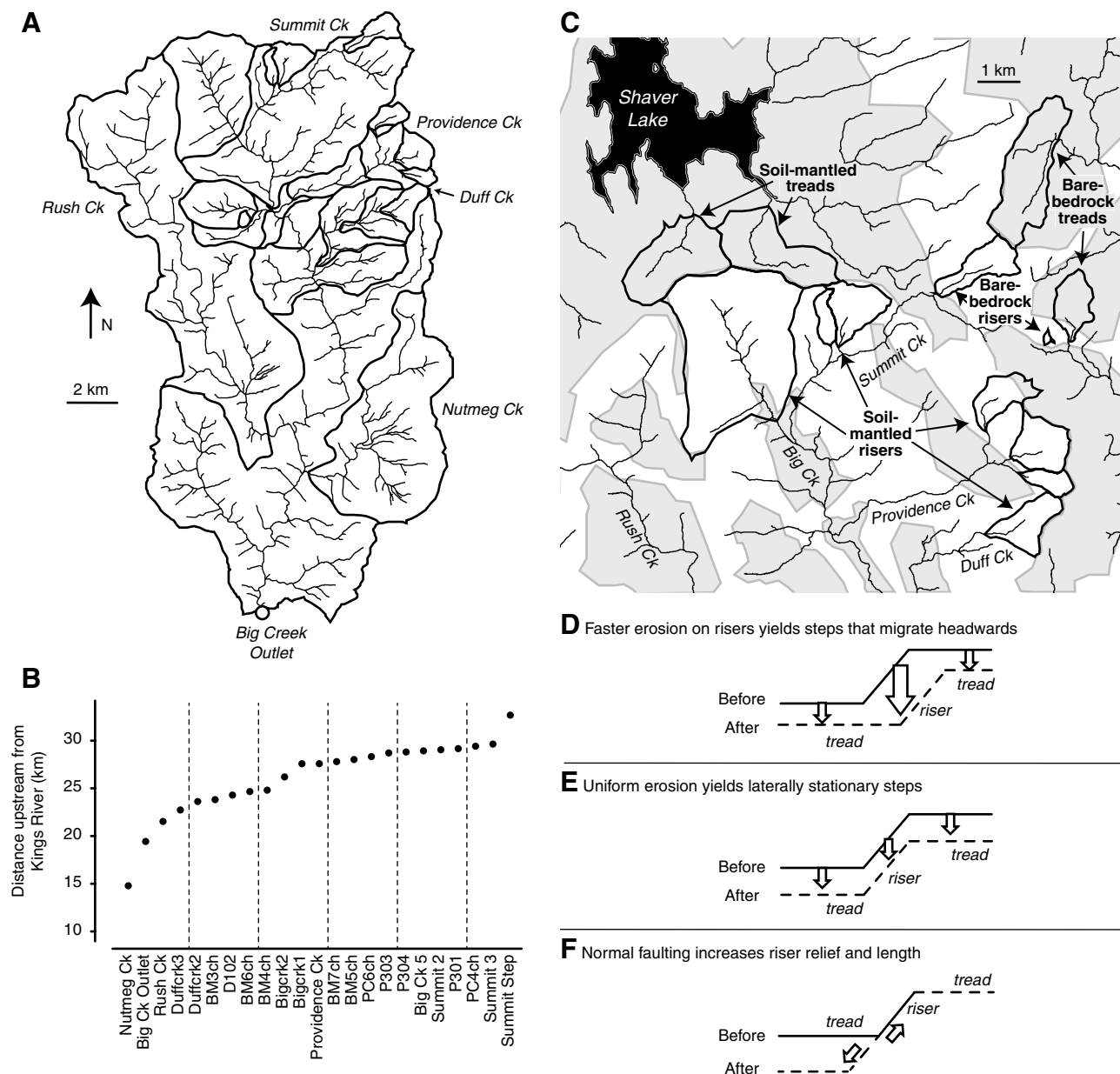
Figure 4. Experimental design. (A) Nested study catchments of Big Creek, which drains a subset of our study area. (B) Range of sampled distances upstream from Kings River base level for the Big Creek catchments. (C) Example illustrating how different elements of the stepped topography were isolated; we sampled areas that drained only bedrock risers, bedrock treads, soil-mantled risers, and soil-mantled treads. Gray shading highlights mapped treads from Figure 2D. (D–F) Conceptual model of stepped topography showing three hypothesized styles of landscape evolution: (D) Faster erosion (thicker arrow) on steep risers causes steps to erode headward toward the range crest; (E) if erosion rates on risers and treads are equal (illustrated by arrows), steps stay in place laterally and erode downward; (F) alternatively, steps may be growing expressions of normal faulting (fault motion shown with arrows) within the western Sierra fault system (after Hake, 1928; Sousa et al., 2016).

whether the Dartmouth and Wyoming data sets can be readily combined without adjustment for biases between laboratories.

Quartz was isolated from sediment and outcrop samples using standard techniques (Kohl and Nishiizumi, 1992). The procedures used by the Wyoming laboratory group were as follows: Purified quartz was spiked with ^{9}Be; dissolved in a 5:1 solution of HF and HNO_3; fumed to dryness in hot (420 °C) H_2SO_4 to remove fluoride complexes; converted to Cl compounds; cleaned of Ti and Fe by raising pH to 14; dissolved in oxalic acid; and subjected to ion exchange chromatography for extraction of Be (PRIME Lab, 2013). The ^{10}Be/^{9}Be ratios of the Wyoming laboratory group samples were measured by AMS at PRIME Lab (Muzikar et al., 2003). Procedures at the Dartmouth laboratory were similar;

following H₂SO₄ fuming, samples underwent column chemistry to extract Be following methods of Ditchburn and Whitehead (1994). The Dartmouth samples were analyzed for $^{10}Be/^9Be$ ratios at CAMS at the Lawrence Livermore National Laboratory (Rood et al., 2010). Process blanks for samples prepared at the University of Wyoming and Dartmouth typically had $^{10}Be/^9Be$ ratios $<6 \times 10^{-15}$ and $<13 \times 10^{-15}$, respectively. We used process-blank–corrected AMS data to calculate ^{10}Be concentrations in quartz using known added masses of ^9Be spikes.

To calculate catchment-averaged erosion rates for each of our study catchments, we used the estimated ^{10}Be concentrations as inputs in the Catchment-Averaged Denudation Rates from Cosmogenic Nuclides (CAIRN) code (Mudd et al., 2016). The CAIRN code is distinguished from previous calculation protocols in that it efficiently incorporates realistic estimates of topographic shielding and cosmogenic nuclide production for an entire catchment using all points extracted from a digital elevation model (DEM). We applied the code to all our catchments, including previously published results that two of this manuscript's coauthors calculated using a different protocol (Hahm et al., 2014). Discrepancies between the CAIRN code and our previous protocol lead to a 9 mm k.y.$^{-1}$ maximum difference in inferred erosion rates for the 25 recalculated erosion rates. To account for production by cosmogenic muons, we selected the Granger and Smith (2000) scaling scheme in the CAIRN code decision tree. We accounted for snow shielding using a local altitudinal trend in snow-water equivalent (California Department of Water Resources, 2013; Hahm et al., 2014) and also included a correction for biomass shielding based on the National Biomass and Carbon data set (Kellndorfer, 2013). Shielding values, ^{10}Be concentrations, and CAIRN calculated rates are shown in Table DR1.[1] Estimates from the CAIRN code were corrected for the effects of chemical erosion in soil-mantled cases using a published empirical relationship between the chemical erosion factor (CEF) and mean annual precipitation (MAP; Riebe and Granger, 2013; Table DR2, see footnote 1). The CEF corrections estimated this way ranged from 1.09 to 1.23 across the sites. This likely underestimates the total erosion rate at sites where deep weathering accounts for most of the chemical depletion observed in soils (Dixon et al., 2009a).

Uranium Isotopes

We collected 27 samples of sediment from streams in the San Joaquin and Kings River watersheds for uranium isotope analysis. Eight of our sites corresponded with cosmogenic nuclide sampling points. In addition, seven of the samples were derived directly from splits of samples collected by the University of Wyoming team for the ^{10}Be analyses described above (Table 1). All uranium (U) isotope sample processing and analyses were conducted at the Wollongong Isotope Geochronology Laboratory, University of Wollongong, Australia. Samples were dried

TABLE 1. SAMPLE SITES GROUPED BY TRIBUTARY CREEK AND MAIN-STEM RIVER

Sample ID	Nuclides measured	Latitude (°N)	Longitude (°W)	Elevation (m)	Mean annual precipitation (cm yr⁻¹)	Average hillslope gradient (m m⁻¹)	Drainage area (km²)	Average distance to outlet (km)
Big Creek, Kings River								
Big Creek 5	$^{10}Be^b$	37.062	119.259	1138	97	0.37	9.24	29
Bigcrk1	$^{10}Be^a$	37.028	119.232	971	98	0.31	50.89	28
Bigcrk2	$^{10}Be^a$	37.016	119.226	947	97	0.31	66.29	26
Big Creek outlet	$^{10}Be^b$	36.916	119.244	306	87	0.30	181.22	19
Bretz Mill Creek, Kings River								
BM3ch	$^{10}Be^a$	37.039	119.255	1055	88	0.20	0.17	24
BM4ch	$^{10}Be^a$	37.039	119.251	1014	91	0.29	3.48	25
BM6ch	$^{10}Be^a$	37.039	119.246	1005	91	0.26	5.36	25
BM5ch	$^{10}Be^a$	37.040	119.245	1000	98	0.32	35.01	28
BM7ch	$^{10}Be^a$	37.037	119.240	998	98	0.31	48.88	28
Bull Creek, Kings River								
B201	$^{10}Be^b$	36.979	119.080	2148	117	0.21	0.54	27
B203	$^{10}Be^b$	36.978	119.074	2190	123	0.20	1.39	28
B204	$^{10}Be^b$	36.977	119.074	2193	122	0.20	1.68	28
Dinkey Creek, Kings River								
BMT01	$^{10}Be^b$	37.096	119.183	2222	112	0.00	0*	39
BMT02	$^{10}Be^b$	37.092	119.179	2213	112	0.00	0*	37
Glen Step 2	$^{10}Be^b$	37.080	119.187	1986	106	0.64	0.00	36
Glen Step 1	$^{10}Be^b$	37.079	119.190	1964	106	0.46	0.04	36
Glen Step 4	$^{10}Be^b$	37.080	119.184	1963	110	0.21	0.97	37
SNS19a	U^c	37.148	119.126	2530	120	0.30	1.14	45
SNS22a	U^c	37.118	119.154	2075	119	0.24	17.41	43
Duff Creek, Kings River								
D102	$^{10}Be, U^e$	37.040	119.204	1486	104	0.33	1.19	24
SNS07	U^c	37.036	119.211	1354	103	0.30	2.13	24
Duffcrk2	$^{10}Be^a$	37.034	119.219	1237	103	0.34	3.36	24
SNS05	U^c	37.034	119.220	1226	100	0.26	5.41	23
Duffcrk3	$^{10}Be, U^d$	37.022	119.227	963	100	0.31	7.07	23
Providence Creek, Kings River								
P304	$^{10}Be^b$	37.052	119.195	1783	103	0.26	0.48	29
PC4ch	$^{10}Be^a$	37.065	119.206	1892	103	0.20	0.74	29
P301	$^{10}Be^g$	37.061	119.204	1791	103	0.21	1.00	29
P303	$^{10}Be^b$	37.056	119.198	1729	103	0.24	1.30	29
PC6ch	$^{10}Be^a$	37.051	119.209	1644	102	0.24	5.14	28
Providence Creek	$^{10}Be^g$	37.043	119.237	1079	101	0.06	7.27	28
Rock Creek, Kings River								
BMT04	$^{10}Be^b$	37.110	119.202	2337	113	0.00	0*	44
BMT05	$^{10}Be^b$	37.110	119.201	2332	113	0.27	0*	44
RC1ch	$^{10}Be^a$	37.129	119.187	2280	117	0.19	0.05	43
RC2ch	$^{10}Be^a$	37.125	119.188	2232	116	0.23	0.22	43
SNS15	U^c	37.106	119.197	2276	115	0.14	0.39	45
SNS16	U^c	37.111	119.193	2252	115	0.15	1.11	44
SNS17	$^{10}Be^g$	37.122	119.187	2224	115	0.17	3.18	43
SNS30	$^{10}Be, U^f$	37.119	119.177	2180	118	0.18	6.18	44
SNS31	$^{10}Be, U^e$	37.118	119.177	2169	116	0.17	11.18	43
SNS32	U^c	37.101	119.169	2076	115	0.17	17.76	42

(*Continued*)

at 60 °C and ground using an agate disc mill. Because our goal was to quantify the U isotope composition of primary and secondary mineral phases derived from parent material, we needed to remove organic matter and allogenic phases precipitated from soil pore waters. To accomplish this, we used a sequential extraction protocol modified from an established technique (Martin et al., 2015). Briefly, we removed any carbonates and exchangeable U and thorium (Th) using sodium acetate; iron oxyhydroxides using hydroxylamine hydrochloride in acetic acid; and organic matter using hydrogen peroxide, nitric acid, and ammonium acetate.

From each sample of leached sediment, we extracted an aliquot that we then weighed and mixed with a measured mass of ^{236}U-^{229}Th tracer solution. The mixture was then dissolved in HF and HNO_3, fumed to dryness, refluxed twice in HNO_3, and then redissolved in 2 mL of 1.5 M HNO_3. Uranium was isolated from the matrix by ion exchange chromatography using established protocols (Luo et al., 1997). The yield was typically >90% for both elements, and 99% of the matrix (i.e., all other elements) was typically removed. Uranium elutions were redissolved in 0.3 M HNO_3 before analysis. Isotopic analyses were performed by multicollector inductively coupled plasma–mass spectrometry on a ThermoFisher Neptune Plus instrument. Samples and standards were introduced using an ESI Apex IR desolvator. The ^{234}U and ^{236}U isotopes were collected in a secondary electron multiplier (SEM) equipped with a retarding potential quadrupole (RPQ), while ^{235}U and ^{238}U were collected in Faraday cups. Typical U blanks were <10 pg, which represents less than 0.01% contribution on measured isotopic ratios. Isotopic ratios were corrected for mass bias and SEM/Faraday yield by analyzing U synthetic isotopic standard NBL U010. The mass bias was calculated by measuring the $^{235}U/^{238}U$ ratio and the SEM/Faraday yield using the mass bias–corrected $^{234}U/^{238}U$ ratio. The tail contribution of ^{238}U on both ^{234}U and ^{236}U was accounted for by analyzing U synthetic standard NBL U010 at the start of each session, and using the ^{238}U intensity of the sample to calculate each tail contribution. Precision and accuracy were estimated from two replicate analyses of U.S. Geological Survey (USGS) reference material QLO-1. Uranium concentration was within recommended values (Table DR3, see footnote 1). In addition, the $(^{234}U/^{238}U)$ activity ratios were close to or at secular equilibrium, as expected. Hereafter, parentheses on isotopic ratios denote activity ratios (i.e., ratios of concentrations times decay constants). The precision of $(^{234}U/^{238}U)$ activity ratios was 0.5%.

TABLE 1. SAMPLE SITES GROUPED BY TRIBUTARY CREEK AND MAIN-STEM RIVER (Continued)

Sample ID	Nuclides measured	Latitude (°N)	Longitude (°W)	Elevation (m)	Mean annual precipitation (cm yr^{-1})	Average hillslope gradient (m m^{-1})	Drainage area (km²)	Average distance to outlet (km)
Summit Creek, Kings River								
SNS11	U[c]	37.091	119.214	1947	109	0.17	0.09	33
SNS14	U[c]	37.094	119.210	2113	111	0.30	0.15	33
Summit 2	^{10}Be[b]	37.078	119.245	1345	98	0.46	0.43	29
SNS12	U[c]	37.092	119.210	2119	115	0.29	0.57	34
SNS13	U[c]	37.094	119.210	2109	115	0.27	0.57	34
Summit Step	^{10}Be, U[f]	37.089	119.218	1849	108	0.35	1.15	33
Summit 3	^{10}Be[b]	37.078	119.243	1341	98	0.45	1.28	30
Miscellaneous tributaries, Kings River								
T003	^{10}Be[b]	36.961	119.027	2050	125	0.26	2.28	26
Nutmeg Creek	^{10}Be[b]	36.959	119.229	448	88	0.36	22.02	15
Rush Creek	^{10}Be[b]	36.970	119.245	593	88	0.25	40.24	21
Dry Creek, San Joaquin River								
BG3ch	^{10}Be[a]	36.954	119.631	145	43	0.17	5.24	16
BG4ch	^{10}Be[a]	36.953	119.631	144	51	0.17	132.81	26
Kaiser Creek, San Joaquin River								
SNS24a	U[c]	37.359	119.175	2200	112	0.26	1.37	24
SNS23a	U[c]	37.319	119.145	2411	122	0.22	20.42	32
SNS27a	U[c]	37.346	119.239	1676	113	0.34	20.65	19
SNS26a	U[c]	37.359	119.241	1633	115	0.24	67.07	26
Rancheria Creek, San Joaquin River								
WB9ch	^{10}Be[a]	37.282	119.087	2962	134	0.13	0.01	33
KR3ch	^{10}Be[a]	37.283	119.107	2613	127	0.26	0.02	31
WB11ch	^{10}Be[a]	37.282	119.088	2959	134	0.12	0.02	33
WB12ch	^{10}Be[a]	37.280	119.091	2915	134	0.14	0.11	32
KR4ch	^{10}Be[a]	37.282	119.109	2572	127	0.33	0.59	31
WB13ch	^{10}Be[a]	37.270	119.102	2586	130	0.31	1.08	31
KR5Ach	^{10}Be[a]	37.278	119.111	2549	128	0.31	1.79	31
Ranch	^{10}Be[a]	37.266	119.118	2507	126	0.25	16.48	31
Ross Creek, San Joaquin River								
SNS62	U[c]	37.245	119.362	1309	99	0.17	0.09	5
SNS61	U[c]	37.235	119.361	1280	102	0.26	5.41	6
SNS60	^{10}Be, U[f]	37.234	119.345	1042	101	0.23	15.93	5
Miscellaneous tributaries, San Joaquin River								
SNS51	^{10}Be[b]	37.364	119.430	2320	123	0.00	0*	21
SNS37	^{10}Be[b]	37.160	119.328	1316	95	0.43	1.04	5
SNS03	U[c]	37.097	119.287	1719	101	0.09	1.42	14
SNS02	U[c]	37.103	119.281	1721	100	0.09	2.65	14
Poison Creek	^{10}Be[b]	37.106	119.262	1662	99	0.11	2.73	15
Swanson Meadow	^{10}Be, U[f]	37.105	119.282	1709	100	0.10	2.87	14
Musik Creek	^{10}Be[b]	37.199	119.309	975	91	0.48	3.58	5
SNS63	^{10}Be, U[f]	37.261	119.356	1415	118	0.21	12.31	8
Saginaw Creek	^{10}Be[b]	37.166	119.417	488	94	0.28	15.77	5
Mill Creek	^{10}Be[b]	37.141	119.382	589	93	0.24	74.79	9

Note: All sample locations correspond to a sampling of stream sediment, except for drainage areas denoted by asterisk, which correspond to point samples of outcrops with negligible drainage area. Superscripts under "Nuclides measured" correspond to different laboratories where samples were processed as follows: a—Dartmouth; b—University of Wyoming; c—University of Wollongong; d—Dartmouth and Wollongong; e—Dartmouth, Wyoming, and Wollongong; f—Wyoming and Wollongong; g—Dartmouth and Wyoming.
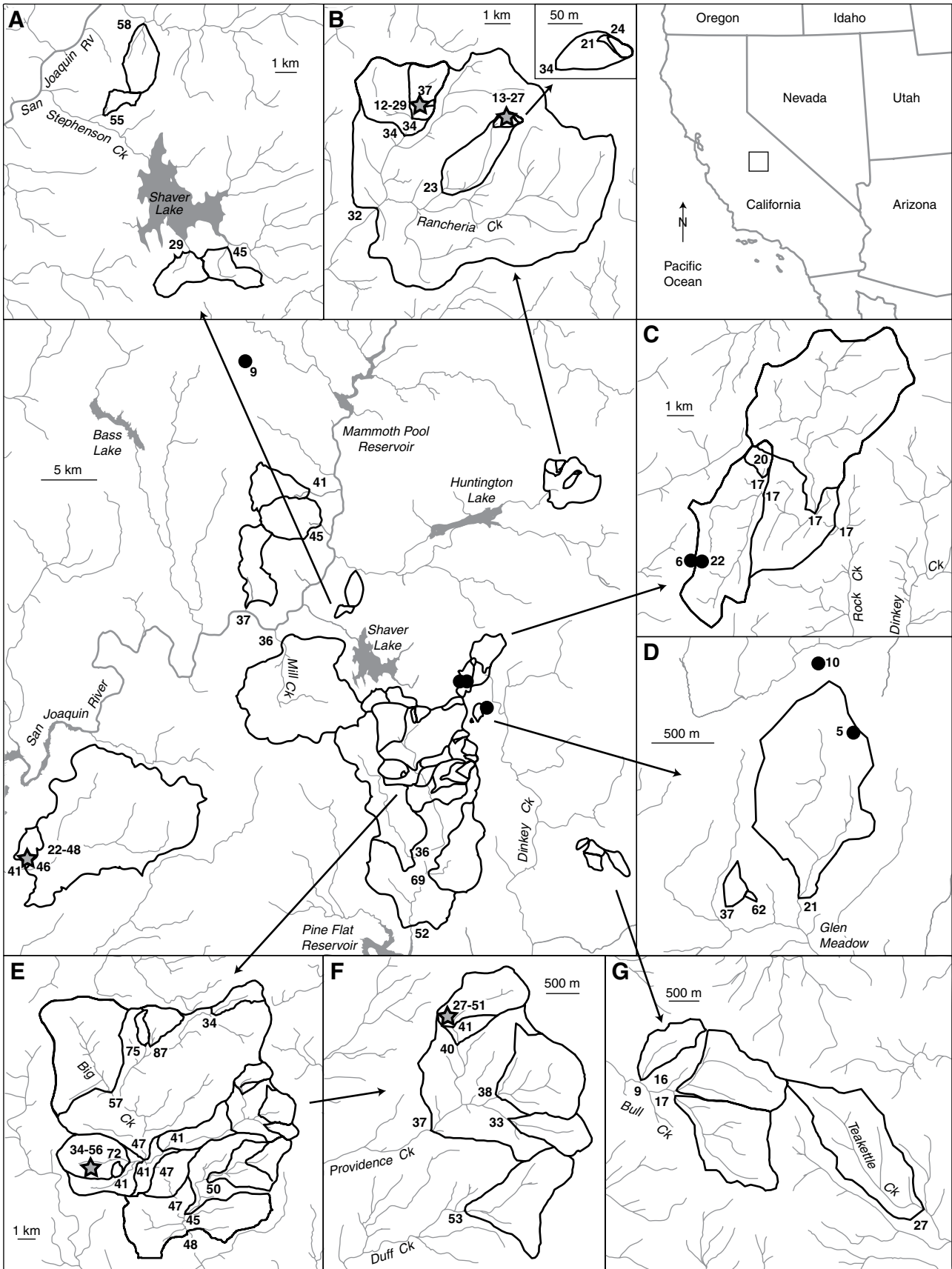
Land Cover

We differentiated the granitic, unglaciated portion of the southern Sierra Nevada landscape into risers and treads using a threshold hillslope gradient of 23%, which we applied to a 10-m-resolution DEM (Fig. 2). We chose 23% as a threshold based on Wahrhaftig's (1965) mapped locations of riser-tread transitions, which typically correspond to a gradient of ~20%–25% (Fig. 2). We applied the 23% gradient threshold and grouped steep and gentle terrain based on connectivity (i.e., whether DEM pixels share an edge) using the Region Group tool in ArcMap

Figure 5.

Geological Society of America Bulletin

10.0. When these regions are plotted on a map of the area, they reveal an alternating sequence of steep risers and gently sloped treads that is broadly consistent with Wahrhaftig's (1965) map of the stepped topography (Fig. 2E). This "region analysis" also allowed us to identify locations of riser-tread transitions, which are key features in Wahrhaftig's hypothesis.

To determine the fraction of bedrock and soil-mantled area in risers, treads, and riser-tread transitions, we used 1-m-resolution, four-band National Agriculture Imagery Program (NAIP) orthoimagery taken in 2009 (U.S. Geological Survey, 2009) and the following manual point-counting protocol. Starting with our hillslope-gradient–based delineation of the risers and treads (wherein we used 23% as a threshold; Fig. 2F), we randomly selected 19 risers, 19 treads, and 16 riser-tread transitions from the broad area of unglaciated granitic terrain in the heart of the stepped topography. Note that these risers, treads, and riser-tread transitions do not correspond to the catchments we selected for the cosmogenic nuclide analyses, such as those shown in Figure 4C. At each of our point-counting sites, we created an ~500 m² polygon that included the selected riser, tread, or riser-tread transition. From each polygon, we randomly selected between 207 and 400 points (i.e., pixels) for land-cover determination by inspection of the corresponding NAIP orthoimagery. In 47 of the 50 polygons, we determined land cover at a minimum of 370 points. For each polygon, we used a manual (i.e., visual) classification approach to group observed land cover into five categories: bedrock; unvegetated soil; vegetated; shadow; and undifferentiated. We then computed the fraction of the identifiable points (i.e., those not mapped as "undifferentiated" or "shadow") that were classified as bedrock, unvegetated soil, or vegetated. In this way, we

generated estimates of the fraction of each element of the stepped topography that is covered by bedrock as well as the fraction covered by vegetation or soil.

Our land-cover analysis likely underestimates bedrock coverage and overestimated soil-mantled and vegetated terrain for at least three reasons: (1) The vegetation canopy can obscure underlying outcrops from view; (2) outcrops <3 m in diameter cannot be confidently identified from the NAIP images; and (3) stained and lichen-covered outcrops are more difficult than bright outcrops to distinguish from surrounding soil-mantled areas. However, as we emphasize in the discussion, these sources of bias would have minimal effect on our analysis if they apply equally to risers, treads, and riser-tread transitions. We therefore argue that our point counting of the NAIP orthoimagery provides first-order estimates of land-cover percentages that are sufficiently robust for our analysis of the distribution of land cover on risers, treads, and riser-tread transitions in the region.

RESULTS

Variations in Erosion Rates from Cosmogenic Nuclides

Our cosmogenic nuclide analyses indicate that erosion rates range from 5 to 87 mm k.y.$^{-1}$ across the study area (Fig. 5; Table DR2, see footnote 1). Five point measurements obtained from drilling into bedrock outcrops on ridges (marked by circles in Fig. 5) range from 5 to 21 mm k.y.$^{-1}$, and thus are generally lower than the catchment-averaged erosion rates, which range from 9 to 87 mm k.y.$^{-1}$. The 31 soil production rates reported in previous work (Dixon et al., 2009a, 2009b) and converted here to equivalent bedrock lowering rates (using a rock density of 2.65 g cm^{-3}) span a 12–56 mm k.y.$^{-1}$ range (marked by stars in Fig. 5). We generally expect soil production rates to be somewhat lower than catchment-averaged erosion rates because they do not include any chemical erosion that occurs below the cosmogenic nuclide production profile (Dixon et al., 2009a), whereas the catchment averages are corrected for deep weathering using the CEF (Riebe and Granger, 2013).

Although catchment-averaged erosion rates vary by roughly a factor of 10 across the entire study area, the range is narrower at finer scales. Likewise, the range in soil production rates is relatively narrow at finer scales. For example, erosion rates of catchments flowing into the San Joaquin River (Fig. 5A) span a 21–58 mm k.y.$^{-1}$ range. Similarly, catchment-averaged erosion rates span a 33–53 mm k.y.$^{-1}$ range, and soil

production rates span a 27–51 mm k.y.$^{-1}$ range in the Providence Creek cluster of the Kings River Experimental Watershed (KREW) group (Fig. 5F). Catchment-averaged erosion rates are slower and span an even narrower range (17–24 mm k.y.$^{-1}$) in catchments feeding Rock Creek (Fig. 5C), which drains a mix of soil-mantled and bedrock hillslopes. The slowest catchment-averaged erosion rates (9–17 mm k.y.$^{-1}$) occur in the Bull Creek catchments (Fig. 5G), which are also part of the KREW group but are distinct among our study catchments in that they are underlain by a metasedimentary roof pendant rather than granitic bedrock (Bateman, 1992).

Replicate measurements of erosion rates from the Wyoming and Dartmouth groups differ by 10% at most (Fig. 6), even though the samples were collected and prepared by two different research teams at two different times and analyzed at two different AMS facilities. Replicate, independent erosion rate measurements such as these are valuable because they are rare (e.g., Balco et al., 2013; Sosa Gonzalez et al., 2017). The similarity in the inferred erosion rates instills confidence that the Dartmouth and Wyoming data sets can be combined without bias, despite any differences in sample collection, preparation, and analysis techniques.
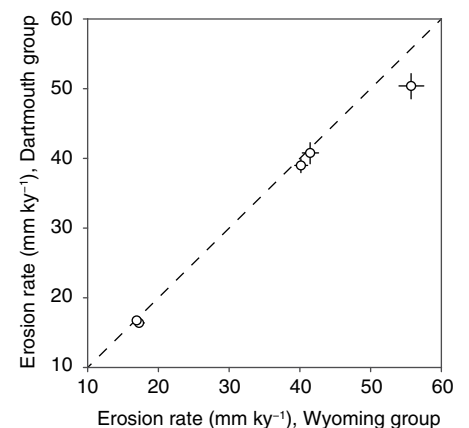
Figure 6. Erosion rates inferred from cosmogenic nuclide concentrations in stream sediment sampled at same locations but two different times and processed at two different laboratories. Erosion rates of samples collected in 2004–2006 and processed at Dartmouth College agree closely with erosion rates of samples collected in 2009–2010 and processed at the University of Wyoming. Error bars include relative error from analytical uncertainty. Measurements from four of the five duplicate analyses agree within one standard error and all of the data lie close to a 1:1 line.
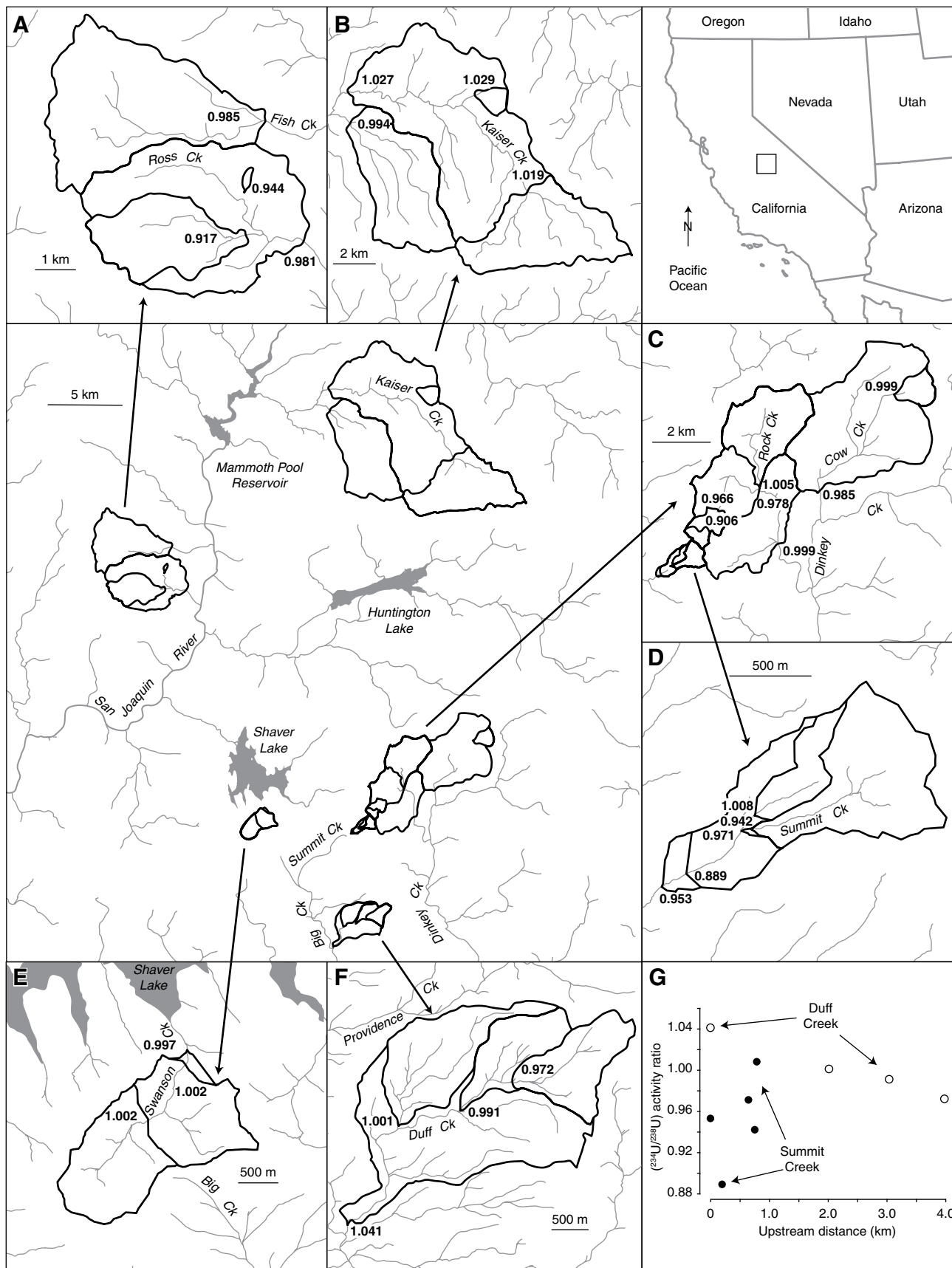
Figure 5. Study area maps showing erosion rates inferred from cosmogenic nuclides. (A–F) Magnification of selected study catchments. Circles indicate erosion rates of bedrock outcrops on hillslopes, and thick black lines indicate catchment boundaries for catchments with areally averaged erosion rates. Gray stars show locations of soil production rate measurements, which were made at varying distances from ridges in several of our study catchments (after Dixon et al., 2009a, 2009b). Gray lines show stream network. Labels near the outlets of the sampled catchments show erosion rate in mm k.y.$^{-1}$ Values near stars show ranges in soil production rates in mm k.y.$^{-1}$.

Figure 7.

Variations in Uranium Isotopic Measurements

Concentrations in U range from 0.43 to 15.71 ppm (median = 1.70 ppm), across the study area (Table DR3, see footnote 1). The $(^{234}U/^{238}U)$ activity ratios in stream sediment range from 0.889 to 1.041 (median = 0.991) across the study area and are reproducible to within 0.005 (Fig. 7; Table DR3, see footnote 1).

Like the cosmogenic nuclide–based erosion rates, the $(^{234}U/^{238}U)$ activity ratios exhibit smaller ranges within clusters of closely grouped catchments. For example, in catchments draining to Rock Creek, $(^{234}U/^{238}U)$ activity ratios range from 0.906 to 1.005 (Fig. 7C). In addition, three of the six clusters of catchments show no systematic trend in $(^{234}U/^{238}U)$ ratios with distance downstream. However, values increase from 0.972 to 1.041 moving downstream along Duff Creek (Fig. 7F), across a series of densely forested soil-mantled catchments. In contrast, they decrease from 1.008 to 0.889 in Summit Creek (Fig. 7D), which drains slopes that are mostly covered in bedrock.

Land-Cover Distribution

Our analysis of land cover in the 54 polled locations yielded the following main results (Table DR4, see footnote 1). In the risers, bedrock surfaces account for an average of just 4% (range: 0%–15%) of the visible polled sites. Meanwhile, in the treads, bedrock surfaces account for an average of only 5% (range: 0%–38%) of the visible polled sites. The transition zones show a similar dominance of soil-mantled and vegetated sites, with bedrock averaging only 5% (range: 0%–34%) of the visible polled sites.

LANDSCAPE EVOLUTION IN THE SOUTHERN SIERRA NEVADA
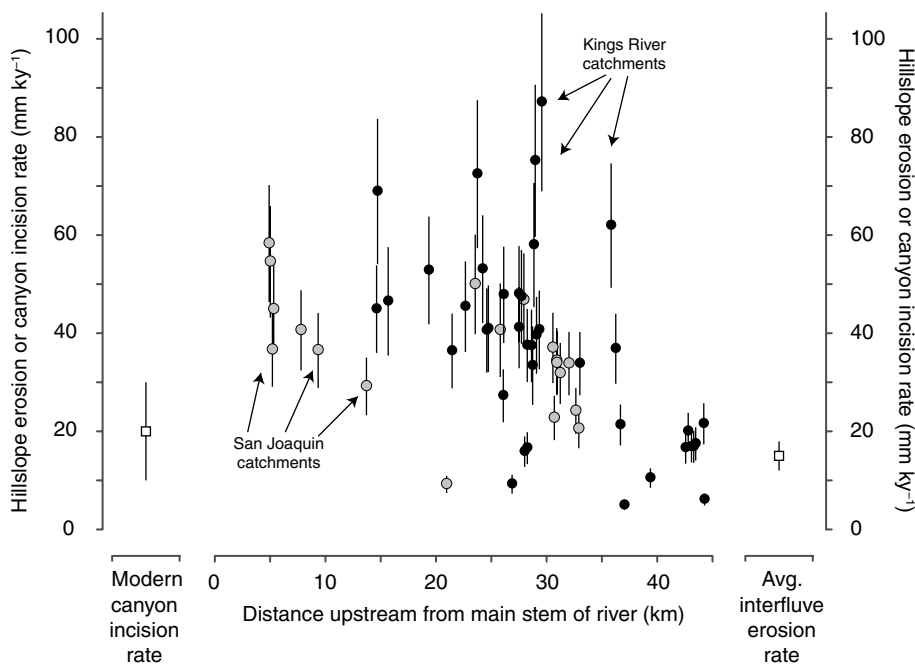
Stability in Canyon-Interfluve Relief

Our data compilation reveals a coherent perspective of landscape evolution in the Si-

erra Nevada. The order-of magnitude decrease in Kings River canyon incision rates from 270 ± 40 mm k.y.$^{-1}$ at 2.7–2.3 Ma to 20 ± 10 mm k.y.$^{-1}$ over the last 320 k.y. (Stock et al., 2004, 2005; Fig. 3) suggests that hillslopes in the region have been responding to marked variations in base-level lowering rates. Meanwhile, erosion rates from the broad interfluves are 17 ± 4 mm k.y.$^{-1}$, averaged over the ~10^4 year time scales encompassed by in situ–produced ^{10}Be accumulation near the surface (Fig. 8). Here, we define interfluves as sites that are in the upper 10th percentile of travel distances to the mainstem canyon of either the Kings River or San Joaquin River canyons. Our average interfluve erosion rate calculation is insensitive to the cutoff percentile; if we chose the 25th percentile instead, we would calculate an average of 20 ± 4 mm k.y.$^{-1}$ We therefore conclude that interfluves are shedding sediment at a rate that agrees within one standard error with the post–320 ka average Kings River incision rate of 20 ± 10 mm k.y.$^{-1}$ (Fig. 7; Stock et al., 2004, 2005), and they are also within two standard errors of the 10 ± 2 mm k.y.$^{-1}$ average interfluve erosion rate reported in previous work (Stock et al.,

2005). This implies that the overall relief (i.e., vertical distance) between the canyons and interfluves has been roughly steady, at least in the lower Kings River basin, for the past few tens of thousands of years. In addition, the spatially distributed erosion rates of catchments between the canyons and interfluves shed new light on relief change in the San Joaquin River basin, despite the lack of measured incision rates for the river over the ~10 k.y. time scales comparable to our erosion rate measurements. In the absence of a statistically significant positive trend between erosion rates and distance upstream from the canyon (gray symbols in Fig. 8), we suggest that, over the broad scale of interfluves and canyons, relief is either steady or increasing over time in the San Joaquin River basin.

Our findings regarding relief change in the region differ from what we might have predicted based on previous studies of detrital thermochronometry, which suggested that relief is growing in the Kings River basin and declining in the San Joaquin River basin (McPhillips and Brandon, 2010). One explanation for the discrepancies is the difference in spatial scale between the thermochronometric and cosmogenic

Figure 7. Study area maps showing stream networks (gray lines) and catchments (black lines) where sediment was collected for U-series disequilibrium analyses. Labels show $(^{234}U/^{238}U)$ activity ratios. (A–F) Selected catchments at higher magnification. (G) Variations in $(^{234}U/^{238}U)$ activity ratios as a function of distance upstream from the sampling point that is furthest from the divide in Summit Creek (Panel D) and Duff Creek (Panel F).

Figure 8. Rates of hillslope erosion and canyon incision from the southern Sierra Nevada. Average hillslope erosion rate of interfluve sites roughly matches modern incision rate of Kings River measured by cosmogenic nuclide burial dating in previous work (Stock et al., 2005). Hillslope erosion rates at intermediate flow distances are more variable than the interfluve erosion rates but nevertheless span a much narrower range than the order-of-magnitude variations in canyon incision rates over time (Fig. 3). Average interfluve erosion rate includes data from this study and Stock et al. (2005).

nuclide data. Although both techniques involve isotopic fingerprinting of modern sediment in streams, and thus average over similar time-scales (Riebe et al., 2015), our samples represent much smaller catchments than the McPhillips and Brandon (2012) study. The detrital thermochronometry samples, taken from the main-stem channels of the Kings and San Joaquin Rivers, with contributing areas of ~4400 and ~5300 km², respectively, include contributions from the rugged, previously glaciated High Sierra (McPhillips and Brandon, 2010). In contrast, the cosmogenic nuclide analyses (used in this study) were more narrowly focused on smaller (0.01–181 km²) tributary catchments that feed only the lower reaches of the Kings and San Joaquin basins. Thus, rather than reflecting an inconsistency in results, the differences may be an expression of variations in relief growth and decline from the lower to upper portions of the drainage basins. Along tributaries of the lower Kings and San Joaquin Rivers, such as Big Creek and Mill Creek (Fig. 5), the overall canyon-interfluve relief is roughly stable. In contrast, across the broader scales of the entire western slope of the range (from the Central Valley to the High Sierra range crest), relief is growing in the Kings River basin and declining in the San Joaquin River basin, as indicated by detrital thermochronometry (McPhillips and Brandon, 2010).

Spatial Variability in Catchment-Averaged Erosion Rates

Figure 8 shows that catchment-averaged erosion rates at intermediate distances (5–43 km) from the basin outlet are more variable (range = 5–87 mm k.y.⁻¹) and, on average, moderately faster (39 ± 9 mm k.y.⁻¹) than both the inter-fluve erosion rates (samples in the upper 10% of travel distances to main stem of either the Kings or San Joaquin Rivers) and the modern Kings River canyon incision rate (17 ± 4 mm k.y.⁻¹ and 20 ± 10 mm k.y.⁻¹, respectively). The variability is small, however, compared to the ~250 mm k.y.⁻¹ drop in the Kings River incision rate from 2.7 Ma to the present (Stock et al., 2004, 2005). This implies that the signal of high canyon incision rates from the early Pleistocene has stalled, it is still propagating through the landscape with a muted amplitude (relative to main-stem incision rate change), or it has finished propagating through the landscape.

The similarity between the interfluve erosion rates and modern river incision rates could be counted as evidence that the signal has finished propagating through the landscape. However, prominent knickpoints in channel profiles of the region (e.g., Fig. 2) suggest that the landscape

has not yet finished adjusting to Pleistocene variations in river incision rates. Additional evidence can be found in longitudinal landscape profiles (Sklar et al., 2016) of four tributaries of Big Creek (Fig. 2D). These landscape profiles exhibit marked convexities (Fig. 2D), confirming patterns implied in the stream profiles (Fig. 2B), i.e., that hillslopes are perched in successively higher steps across the landscape (Crosby et al., 2007). The tops of the risers correspond to convexities in the channel profile (Fig. 2B), which serve as local base levels for the treads upstream, which are represented in Figure 2D as the perched hillslopes. Together, the convexities in the channel and landscape profiles imply that the perched hillslopes have not yet adjusted to Pleistocene variations in canyon incision rates. This means that each successive tread along a path from the canyon to the interfluve is adjusted to a successively older base level (e.g., Crosby and Whipple, 2006). This further implies that the similarity between the interfluve erosion rates and canyon incision rates is a coincidence rather than an outcome of landscape adjustment to Pleistocene variations in base-level lowering rates.

Controls on Erosion Rate Variability

Between the interfluves and the canyons, the spatial variability in erosion rates can be explained by variations in topography and land cover. Erosion rates increase with hillslope gradient across both soil-mantled and bedrock catchments (Fig. 9), raising the possibility that steep risers are eroding faster than—and thus migrating laterally into—gentle hillslopes on the treads above them (Fig. 4D). This would be inconsistent with Wahrhaftig's (1965) hypothesis that the combination of bedrock risers

Figure 9. Erosion rate vs. gradient for bedrock (open symbols) and soil-mantled terrain (closed symbols) in granitic bedrock of the southern Sierra Nevada (Table 1).

below soil-mantled treads results in laterally stable steps (Fig. 4E), if the presence of soil and bedrock modulates the erosion rates (Granger et al., 2001). To more conclusively evaluate Wahrhaftig's (1965) hypothesis, we chose a subset of catchments that isolate individual risers and treads (as shown in Fig. 4C) for an analysis of variance (ANOVA) of erosion rates (Table DR5, see footnote 1). Based on field observations of the dominance of soil and bedrock (e.g., Hahm et al., 2014), we further classified risers and treads into soil-mantled and bedrock categories, recognizing that they typically erode at different rates in granitic landscapes (Fig. 3B). Thus, our subset eliminates catchments that span multiple risers and treads and eliminates catchments that have mixtures of bedrock and soil-mantled hillslopes. Either of these mixtures could confound our ability to evaluate the hypotheses about lateral migration and stability of the steps.

The ANOVA of erosion rates from the stepped topography indicates that bedrock treads are eroding significantly slower than catchments in the three other categories (Fig. 10; see Table 2 for significance levels). However, the mean erosion rates of soil-mantled risers, soil-mantled treads, and bedrock risers are statistically indistinguishable from each other according to a Tukey honestly significant difference (HSD) test (Table 2). This is consistent with Wahrhaftig's (1965) hypothesis about the lateral stability of the steps (Fig. 4E).

Transport-Limited versus Weathering-Limited Erosion

Uranium isotopes can be used to quantify the relative role of physical versus chemical erosion on the risers and treads. When uranium isotopes fractionate at mineral surfaces, a fraction of ²³⁴Th produced by decay of ²³⁸U can be recoiled into the surrounding medium. The recoiled ²³⁴Th then decays into ²³⁴U, resulting in a depletion of ²³⁴U compared to ²³⁸U within 20–30 nm of the mineral surface. As mineral size is reduced by physical and chemical weathering, a ²³⁴U-²³⁸U radioactive disequilibrium develops in regolith. This disequilibrium increases over time, resulting in decreasing (²³⁴U/²³⁸U) activity ratios in regolith. This property has been used to quantify the rates of soil production (Dequincey et al., 2002; Dosseto et al., 2008b) and fluvial sediment transport (Dosseto et al., 2008a, 2010; Granet et al., 2010; Dosseto and Schaller, 2016) in recent studies around the world. Here, it is postulated that the uranium isotope composition of sediments could record the relative efficiency of physical and chemical weathering processes in breaking down mineral grains.
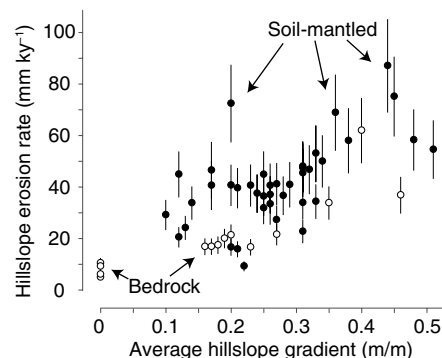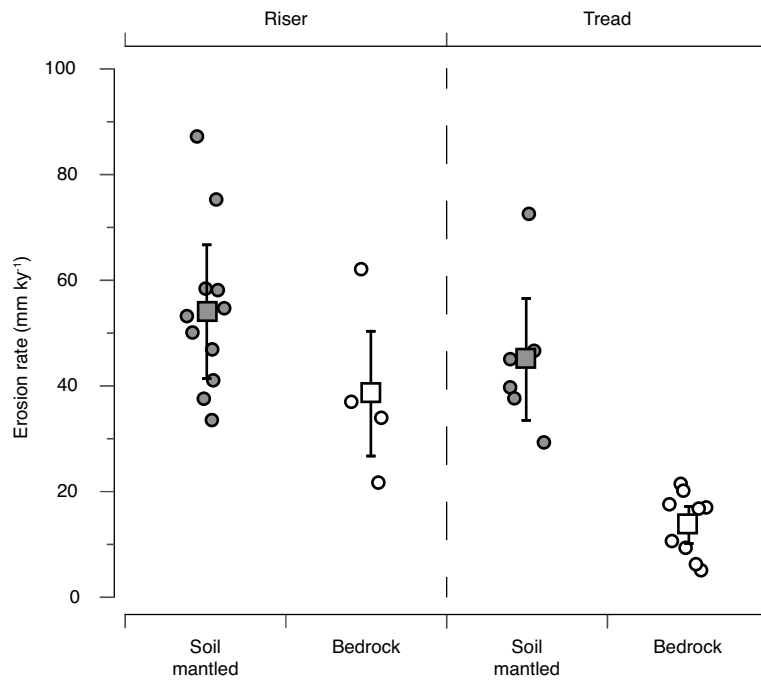
Figure 10. Erosion rates grouped by land-cover and landscape type. Analysis of variance (ANOVA) shows that bedrock treads are eroding slower on average than the other three groups, implying that combinations of either soil-mantled or bedrock risers in front of bedrock treads should lead to headward migration of the treads. All other riser-tread combinations are laterally stable on average.

et al., 2014; Attal and Lavé, 2009). Hence, the finding that (^{234}U/^{238}U) activity ratios are lower where soil is absent (vs. where soil is present) is consistent with higher physical weathering on bedrock slopes, which is also consistent with regolith production on these features being weathering-limited. The variations in (^{234}U/^{238}U) activity ratios across the additional subgrouping of risers and treads (Fig. 11B) are less pronounced and moreover do not exhibit a statistically significant difference in the ANOVA across the four landscape categories (Table 2). Nevertheless, the (^{234}U/^{238}U) activity ratios, when broadly grouped, are consistent with a dominance of weathering limitations in bedrock catchments and transport limitations in soil-mantled catchments.

Erosional Equilibrium in the Stepped Topography

Together, the cosmogenic nuclide and uranium isotope data are broadly consistent with Wahrhaftig's (1965) proposed weathering-related mechanism for lateral stability of the steps. However, while our study catchment selection allows us to quantify representative erosion rates for each land-cover and landscape type (Fig. 4C), they do not reveal their frequency of occurrence on the landscape. Therefore, they do not test the assertion that the most common combination of landscape categories in the stepped topography is bedrock risers next to soil-mantled treads—a central aspect of Wahrhaftig's hypothesis. To quantify the prevalence of this combination, we used our observations of land cover on randomly selected risers, treads, and riser-tread transitions (Table DR4, see footnote 1). They indicate that bedrock is rare on all features, including risers (Fig. 12). This provides a crucial refutation of Wahrhaftig's hypothesis, implying that bedrock risers in front of soil-mantled treads are much less common than needed for Wahrhaftig's mechanism to dominate landscape evolution in the region. Only one of the risers in our random sampling had more than 10% exposure of bedrock. Moreover, in our study site selection for the cosmogenic nuclide and uranium isotope analyses (Figs. 10 and 11), we found only four and five suitable examples, respectively, of bedrock risers in the region (Table 2). Bedrock exposures were also infrequent at the transitions between risers and treads, where, according to Wahrhaftig, weathering limitations on erosion would be an especially crucial control on base level for the adjacent tread (Fig. 12). Instead, soil covers at least 90% of the visible landscape in 18 out of 19 risers, 18 out of 19 treads, and 14 out of 16 riser-tread transitions. This implies that the most common

Uranium isotopic compositions are broadly consistent with the proposed weathering and transport limitations on erosion of bedrock and soil-mantled hillslopes, suggesting that at least some of the observed erosion rate differences may be driven by differences in regolith production processes. The (^{234}U/^{238}U) activity ratios in stream sediment are significantly lower

in bedrock versus soil-mantled catchments ($p = 0.03$; Table 2; Fig. 11A). One mechanism for the preferential depletion of ^{234}U over ^{238}U is via recoil ejection of ^{234}U from silt-sized sediment particles (Kigoshi, 1971). Production of silt-sized particles in mountain streams is thought to be dominated by physical processes such as abrasion and grain-to-grain impacts (Miller

TABLE 2. RESULTS OF TUKEY'S HONESTLY SIGNIFICANT DIFFERENCE (HSD)
TEST FOR DIFFERENCES BETWEEN GROUPS OF ^{10}Be AND (^{234}U/^{238}U) DATA

Comparison (number in parentheses)	Difference ± std. error	Tukey's q	Significance level (p)
^{10}Be-based erosion rates			
Soil-mantled risers (11) vs. bedrock treads (9)	40.4 ± 6.1 mm k.y.$^{-1}$	6.64	<0.0001
Bedrock risers (4) vs. bedrock treads (9)	24.9 ± 8.1 mm k.y.$^{-1}$	3.06	0.02
Soil-mantled risers (11) vs. soil-mantled treads (6)	9.0 ± 6.9 mm k.y.$^{-1}$	1.32	0.56
Bedrock risers (4) vs. soil-mantled treads (6)	6.5 ± 8.7 mm k.y.$^{-1}$	0.74	0.88
Soil-mantled terrain (17) vs. bedrock terrain (13)	29.5 ± 5.7 mm k.y.$^{-1}$	5.15	<0.0001
(^{234}U/^{238}U) activity ratios			
Soil-mantled risers (8) vs. bedrock treads (5)	0.034 ± 0.019	1.76	0.32
Bedrock risers (5) vs. bedrock treads (5)	0.018 ± 0.021	0.85	0.83
Soil-mantled risers (8) vs. soil-mantled treads (9)	0.022 ± 0.016	1.31	0.56
Bedrock risers (5) vs. soil-mantled treads (9)	0.031 ± 0.019	1.61	0.39
Soil-mantled terrain (17) vs. bedrock terrain (10)	0.032 ± 0.014	2.32	0.03
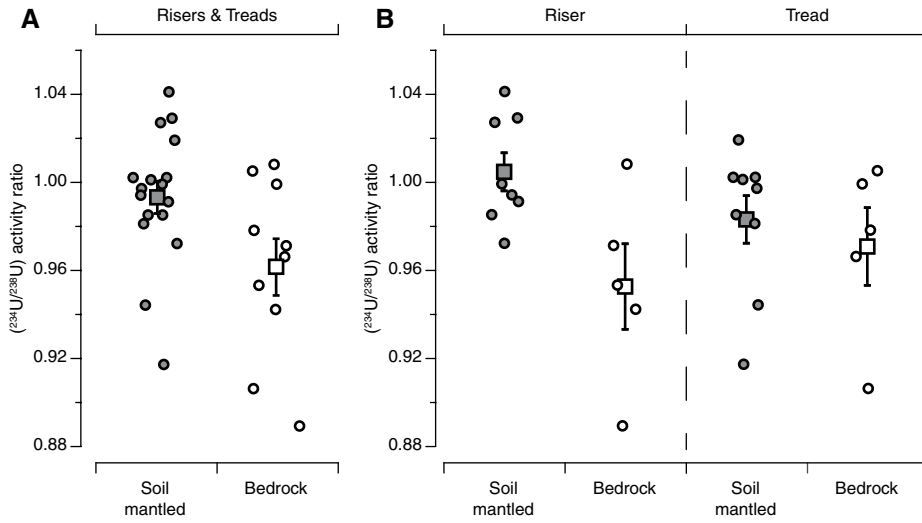
Figure 11. (A) Uranium isotope activity ratios are higher in soil-mantled catchments on average than they are in catchments dominated by bedrock. (B) When data are grouped by landscape type as well as land cover, the analysis of variance (ANOVA) is unable to detect significant differences in (^{234}U/^{238}U) activity ratios among the groups.

arrangement of individual steps in the stepped topography is a soil-mantled riser in front of a soil-mantled tread.

The Tukey HSD test, described earlier, shows no statistically significant difference between the erosion rates of the soil-mantled risers and treads (Table 2). When coupled with the land-cover analysis of Figure 12, this indicates that most of the steps in the southern Sierra Nevada are laterally stable (Fig. 4E), consistent with Wahrhaftig's (1965) conclusion that the steps are eroding in dynamic equilib-

rium, with little or no lateral retreat toward the range crest. However, Wahrhaftig's proposed mechanism—in which weathering limitations on steep, bedrock risers conspire with transport limitations on soil-mantled treads to promote spatially uniform erosion rates—does not commonly play a role in the lateral stability of the stepped topography. Instead, the stability can be largely explained by the lack of variability in erosion rates across the soil-mantled risers and treads. This may seem paradoxical given the apparent continuous increase in erosion rates with increasing gradient in soil-mantled terrain (Fig. 9). However, many of the intermediate rates in Figure 9 include combinations of multiple risers and treads, which give the catchments intermediate gradients and make them ill-suited for determining retreat rates of individual steps. Our analyses of isolated risers and treads, and the grouping by land-cover type, however, should provide an analysis that is matched in scale to step retreat and thus can provide realistic rates of this process.

As shown in Figure 12, there are two uncommon combinations of landscape categories to consider in evaluating the potential for temporal changes in the position of riser-tread transitions in the southern Sierra Nevada: bedrock treads fronted by soil-mantled risers, and bedrock treads fronted by bedrock risers. Both have statistically significant differences
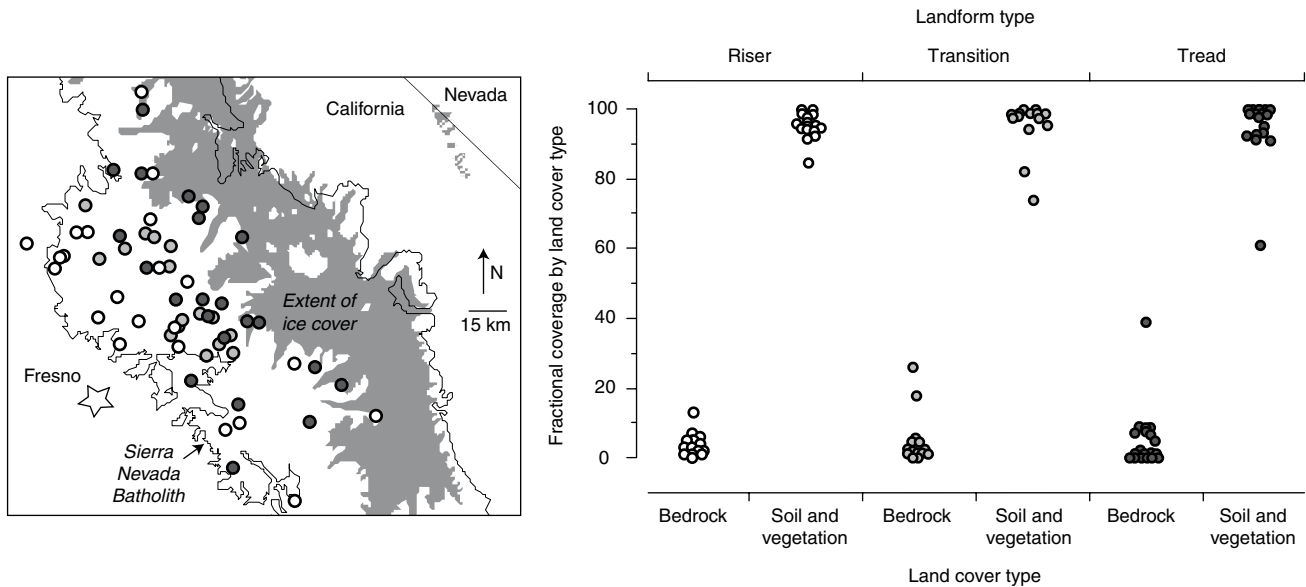
Figure 12. Land-cover polling locations and data. (Left) Locations of randomly selected risers (white), treads (dark gray), and riser-tread transitions (light gray) in the southern Sierra Nevada Batholith (thin outline) lie outside the limits of Pleistocene ice advance (gray shaded area). (Right) Fractional coverage of visible area by land-cover types quantified using point counting protocol. Coverage by bedrock is typically less than 10%, even on steep risers, a finding that is inconsistent with Wahrhaftig's (1965) hypothesis about formation of the steps.

Geological Society of America Bulletin

in erosion rates, with the risers eroding faster than the treads according to the Tukey HSD tests (Table 2). This implies that these types of steps are migrating toward the range crest, as illustrated in Figure 4D. The migration rate can be quantified using geometric arguments following Penck (1924). For a planar tread with gradient α above a planar riser with gradient β, if the tread and riser are lowering at rates E_{tread} and E_{riser}, respectively, the horizontal headward migration velocity (v) of the riser can be written as $v = (E_{riser} − E_{tread})/(β − α)$. Given the largest discrepancies between measured mean erosion rates on treads and risers (E_{riser} = 54 mm k.y.$^{-1}$ for soil-mantled risers and E_{tread} = 14 mm k.y.$^{-1}$ on bedrock treads on average; Fig. 10) and field-derived values for the gradients (~0.36 m/m for the risers and ~0.11 m/m for the treads on average; Fig. 2E), this expression implies a headward migration rate of ~160 mm k.y.$^{-1}$ for the riser, and thus ultimately for the knickpoint that defines it (Figs. 2B and 2D). At this rate, it would take ~56 m.y. for the main riser of Figure 2F to erode headward through the 9-km-wide tread shown in the middle of the map. This rough calculation shows that, even for regions of the stepped topography that are out of erosional equilibrium, the risers are currently migrating headward so slowly that the steps should persist for many millions of years—far longer than the ~10^5 year period of the glacial-interglacial cycles that may have driven variations in river incision rates in the Sierra Nevada. The migration rate calculated here represents a maximum rate. The only other statistically distinguishable riser-tread combination (bedrock treads fronted by bedrock risers) has a smaller difference in mean erosion rate, yielding an estimated migration rate of only ~80 mm k.y.$^{-1}$

Arrested Development due to a Paucity of Coarse Fluvial Sediment

Collectively, our observations suggest that landscape evolution in our study area is in a state of arrested development. Overall relief between interfluves and canyons is not currently growing or shrinking (Fig. 8), despite an order of magnitude of variation in canyon incision rates over the Pleistocene (Fig. 3A). Hillslope erosion rates in catchments with intermediate travel distances are somewhat higher than the canyon and interfluve rates, suggesting that these areas are lowering faster and thus slowly creating concavity between the canyons and interfluves. However, these rates span a much narrower range than the Pleistocene variations in canyon incision rates, inconsistent with the transient passage of erosion signals through the landscape. The numer-

ous convexities in the landscape (Fig. 2D) and stream channel profiles (Fig. 2B)—which might otherwise be interpreted to reflect ongoing landscape adjustment to transient incision signals—are migrating headward very slowly or not at all. This implies that any incision signals from base-level lowering in the canyons have largely stalled. However, the mechanism proposed by Wahrhaftig (1965)—i.e., that weathering and transport limitations conspire to produce uniform erosion across risers and treads—does not provide a satisfactory explanation for the arrested development, because bedrock risers are too rare in the ubiquitous stepped topography.

This raises the question: If Wahrhaftig's mechanism cannot explain the stability of the steps, what can? One possibility is a paucity of coarse sediment in channels, and thus a lack of tools essential for cutting down through bedrock channels (Sklar and Dietrich, 1998, 2001; Whipple et al., 2000; Cook et al., 2013; Turowski et al., 2015). This would inhibit headward migration of bedrock knickpoints and prevent any signals from propagating through the channel network (Brocard et al., 2016), consistent with our observations.

A tools limitation on knickpoint migration is supported by several lines of evidence from both hillslopes and channels. Weathering profiles visible in road cuts (Fig. 13A) and imaged in seismic refraction surveys are 6–43 m thick and increase in thickness with increasing elevation (Klos et al., 2018). These thicknesses imply regolith residence times of 0.2–1.0 m.y. (Fig. 13B) when paired with soil production rates from cosmogenic nuclides (Fig. 3C). (Here, we calculated regolith residence times by dividing regolith thickness by the average soil production rate [Riebe et al., 2017].) Weathering is sufficiently intense (Dixon et al., 2009a) and residence times are sufficiently long (Fig. 13B) to produce mostly fine-grained sediment by the time material is exhumed through saprolite and converted to soil (Graham et al., 2010). This is evident in soils in the Providence Creek area (Fig. 13C), which contain a high percentage of sand and fine gravel (Fig. 13D). Grain-size data from stream channels also show an abundance of fine sediment on gently sloped glides (Fig. 13E). Some coarser sediment enters the main channel at junctions with steep tributary streams (Fig. 13F), but this material does not apparently get transported through the glides to the knickpoints (cf. black and green lines in Fig. 13F).

From these observations, we hypothesize that, as creeks wind across the low-gradient treads, they primarily receive sand-sized and finer sediment because of deep and prolonged weathering on adjacent hillslopes (Figs. 13A–

13D). Any coarse sediment that is supplied from steeper slopes at the upstream edge of the tread is lost from the sediment flux during transport to the downstream knickpoints (Fig. 13F). These losses occur due to low transport capacity in the gentle glides (Fig. 13E), leading to preferential transport of finer sediment (Paola et al., 1992), which in turn causes longer in-channel residence times that promote chemical weathering and granular disintegration of coarser sediment (Heller et al., 2001; Sklar et al., 2006; Goodfellow et al., 2016).

An additional line of evidence for limited supply of coarse sediment is the presence of bare bedrock in the channel bed both at and immediately downstream of tread-to-riser transitions (Fig. 13G). Most of the prominent knickpoints are characterized by exposed bedrock cascades that likely only erode via abrasion when coarse sediment is entrained in the channel flow (Sklar and Dietrich, 2004). However, in most reaches immediately upstream of the knickpoints, we observe long, low-gradient, sand-bedded glides like the one shown in Figure 13E. Thus, even when flows are high enough to mobilize bed material, the sediment load is likely dominated by sand and very fine gravel (<10 mm), which travel primarily in suspension over the bedrock knickpoint without causing much abrasion of the bed (Sklar and Dietrich, 2004; Lamb et al., 2008; Scheingross and Lamb, 2016). Moreover, the bedrock channel bed at many of the knickpoints is dominated by potholes, which we interpret as indicative of low coarse sediment supply relative to local transport capacity (Sklar and Dietrich, 2004). Potholes form when a small number of "grinder" clasts are trapped in a depression and repeatedly circulate, abrading the pothole floor and walls (Springer et al., 2005). If there had been a high flux of coarse sediment through the reach, nascent potholes would have filled with sediment, and abrasion of rock between potholes would have led to breaching, coalescence, and ultimately the destruction of the potholes (Wohl et al., 1999). Instead, we find numerous well-developed potholes, mostly empty, with a few abrasive tools trapped at the bottom (Fig. 13I). Together, these observations from both hillslopes and channels support our hypothesis that a lack of coarse sediment supply to bedrock knickpoints is responsible for the arrested development of the landscape.

Alternative Explanations for Arrested Development

While we favor the paucity-of-tools hypothesis described above, other mechanisms may have contributed to the stalled evolution of the stepped topography. For example, one
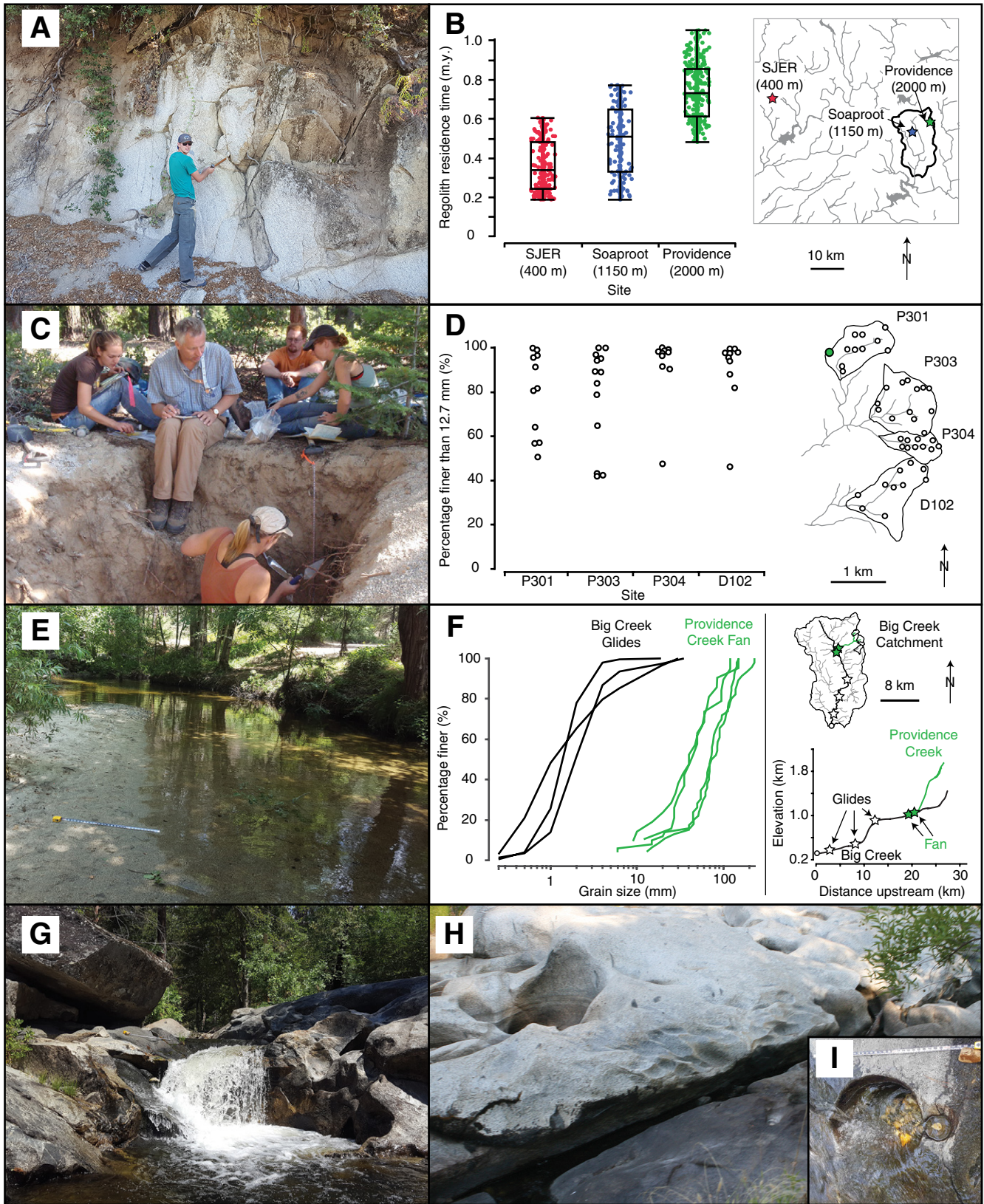
Figure 13.

Figure 13. Field evidence of sediment starvation at knickpoints in the southern Sierra Nevada. (A) Road cuts in the region expose thick profiles of highly weathered regolith that disintegrates to grus with minimal physical disruption. (B) Regolith residence time at three elevations across the southern Sierra Nevada. Residence time was calculated by dividing thickness by average soil production rate at each elevation (Dixon et al., 2009a, 2009b). Thickness was quantified as depth to 4 km/s velocity contour (Flinchum et al., 2018) of P-wave tomography models from seismic refraction surveys (Holbrook et al., 2014; Klos et al., 2018). Low elevation site is located within the San Joaquin Experimental Range (SJER), which is climatically similar to the Dry Creek sites considered in the cosmogenic nuclide analyses (Table 1). (C) Sampling a soil pit in the P301 catchment (green symbol, inset). (D) Percentage of fine sediment in soil pits in P301, P303, P304, and D102 (Johnson et al., 2011; Table DR6 [see text footnote 1]). Data suggest that hillslopes are mostly producing sand and fine gravel. (E) A glide on a Big Creek tread, near the upstream edge of a knickpoint, showing the gentle slope of the bed and paucity of coarse bed sediment. (F) Grain-size distributions from glides along Big Creek (red) and riffles on Providence Creek fan (green; see also Table DR6 [text footnote 1]). Lack of coarse sediment in glides suggests that the coarser sediment is not being transported across the gentle glides. Stars represent sampling locations on map and drainage network long profile (insets). (G) At low flow, a small waterfall defines the top of a knickpoint downstream of glide shown in panel E. Measuring tape at rim of waterfall is 1 m. (H) Fluted and pothole-scarred bedrock on Big Creek. Large pothole at left is ~1 m diameter. The surface is elevated above bedrock slot containing base flow during summer dry season. (I) Pothole with a few coarse sediment particles at waterfall in B, further suggesting a paucity of coarse sediment supply and transport within the reach. Collectively, these observations support the argument that river incision is limited by a paucity of abrasive tools at knickpoints due to size reduction of sediment during weathering of regolith on hillslopes and transport of sediment across gentle glides.

possibility is that the knickpoints have stalled due to lithologic variations in the channel bedrock. Relatively resistant bedrock can interrupt upstream transmission of base-level lowering, leading to production of a knickpoint (Miller, 1991). Higher resistance might arise due to lower fracture density or from a mineralogy that makes the bedrock more durable. Alternatively, differences in bedrock mineral composition could drive differences in chemical weathering of exposed bedrock at knickpoints, making some of it less prone to abrasion (Murphy et al., 2016). Another possibility is that spatial variations in fracture spacing could determine whether high-stage flow in the river is able to entrain bedrock blocks from the channel bed, and thus whether knickpoints are able to migrate through reaches with wide fracture spacing (DiBiase et al., 2015). Our field observations suggest that the fracture spacing in channels is wide wherever bedrock is exposed, including at knickpoints. In addition, mapped locations of geologic contacts do not match the spatial distribution of the knickpoints and steps (Wahrhaftig, 1965; Bateman, 1992). This suggests that variations in lithology cannot adequately explain the arrested development. However, because we lack quantitative data on the spatial distribution of fracture spacing, we are not able to conclusively test hypotheses about lithologic control of the stepped topography.

Yet another possibility is that the paucity-of-tools mechanism is modulated by lithologic effects on the size, supply rate, and strength of abrasive tools from hillslope erosion. A recent study of controls on forest cover in the region showed that transitions between bedrock and soil-mantled terrain often coincide with the contacts between granitic plutons of differing composition, with nutrient-poor bedrock underlying slopes with low forest canopy cover (Hahm et al., 2014). If the size distribution of sediment supplied to channels is a key regulator of channel incision (Sklar et al., 2017) and is furthermore coupled to variations in forest cover, as seems to be the case elsewhere in granitic terrain of the Sierra Nevada (Riebe et al., 2015), then the observed lithological control of forest cover (Hahm et al., 2014) could play a role in the persistence of bedrock knickpoints in the channel. More work is needed to test this hypothesis about feedbacks between bedrock composition, sediment supply, and channel incision (Sklar et al., 2017).

The paucity-of-tools mechanism may also be modulated by climate change, which at our site has included multiple glacial-interglacial transitions over the time scale spanned by the Pleistocene variations in incision rates (Fig. 3A). Although most of our study area was outside

the limits of Pleistocene glaciation (Fig. 1), our sites are close enough to the maximal ice margins that the production of sediment was likely influenced by periglacial conditions for extended periods. This is particularly true for middle elevation sites near the maximal ice margins, for example, in the headwaters of Big Creek (Fig. 5). This could have led to marked changes in erosion rates (Marshall et al., 2015) and the degree of weathering of sediment produced on hillslopes (Schachtman et al., 2016). These changes would have had difficult-to-evaluate effects on both the size distribution and flux of sediment supplied from hillslopes to channels. The potential influence on the position of knickpoints in the channel network is therefore also difficult to evaluate (e.g., Whipple and Tucker, 2002; Whipple, 2004; Sklar and Dietrich, 2004).

Quaternary cycles in climate could also modulate incision rates on the main-stem rivers, which have received sediment from the previously glaciated High Sierra. During glacial periods, a high sediment flux could cause aggradation, thus reducing exposure of the channel to river incision processes (Hancock and Anderson, 2002). In contrast, during interglacial periods, the aggraded sediment would be removed, and incision rates would presumably be accelerated by the enhanced flux of abrasive tools. While this mechanism may modulate river incision and hillslope erosion on the main stem, it cannot explain the slow erosion rates and abundant knickpoints in the unglaciated catchments considered here. In addition, we can largely rule out the influence of accelerated erosion due to periglacial processes (e.g., Marshall et al., 2015) as a factor in time-varying incision because our highest-elevation sites (which would be most prone to periglacial processes) have the slowest erosion and also integrate erosion over the longest time intervals (i.e., at least one glacial-interglacial cycle).

In addition to changing over time, climate at any given moment can vary with distance from the main-stem channel as a function of elevation. Climatic differences could affect incision rates directly by influencing erosional efficiency (e.g., Ferrier et al., 2013) or indirectly by influencing weathering (and thus resistance to incision) at exposed bedrock surfaces that define the knickpoints (Murphy et al., 2016). Altitudinal variations in climate can also drive down-valley variations in the size distribution and flux of sediment produced by hillslope erosion, as suggested recently in a catchment draining the east side of the Sierra Nevada (Riebe et al., 2015; Lukens, 2016). This may also be a factor across our study area on the western slope (Fig. 1). Hillslopes at lower elevations have thinner

Geological Society of America Bulletin

regolith (Klos et al., 2018) despite having similar soil production rates (Fig. 3C), implying shorter residence times (Fig. 13B) and thus less potential for sediment size reduction during regolith production and subsequent weathering (Riebe et al., 2015; Sklar et al., 2017). Thus, tributary channels at lower elevations could have a coarser sediment supply, perhaps even with stronger particles (Goodfellow et al., 2016), capable of more efficient bedrock channel incision (Sklar and Dietrich, 2001), simply because of the lower regolith residence times that seem to prevail there.

One final possibility to consider—but one that cannot be fully assessed at this time without additional observations—is that the distribution of knickpoints and stepped topography reflects the role of normal faulting across the landscape (Fig. 4F). The idea that the steps represent growing expressions of the western Sierra fault system has gained renewed attention (Sousa et al., 2016) after emerging almost a century ago (Hake, 1928), thanks to new thermochronometric constraints on fault structure (Sousa et al., 2016, 2017). For example, marked differences in thermochronometric age over short distances on slopes have demonstrated that at least some of the more pronounced and linear steps of Wahrhaftig (1965) are a result of normal faulting within the range (Sousa et al., 2016). More age constraints are needed to determine whether the smaller, more irregular steps, such as the ones mapped in Figure 2, could be partly explained by faulting.

Conceptual Model of Origin and Arrested Development of the Stepped Topography

We speculate that the initial advance of ice in the range, ~2.5 m.y. ago, contributed to rapid sculpting of the glacial landforms that now dominate the high country, as initial Pleistocene ice advances have done in other mountain ranges around the world (Shuster et al., 2005). This would have contributed abundant coarse sediment supply to main-stem rivers, such as the Kings and San Joaquin Rivers, and thus in turn may have aided rapid incision of bedrock channels. However, some rock uplift within the canyons was needed to drive base-level lowering and subsequent erosion of bedrock channels (Stock et al., 2005). The plausible flexural isostatic response to erosion in the High Sierra and deposition in the Central Valley (e.g., Small and Anderson, 1995) is insufficient to account for the needed rock uplift along the channels, as noted by Stock et al. (2005). Hence, without some tectonically induced base-level lowering, the canyons would have simply acted as conduits (or even aggradational choke points) of

sediment in transit from High Sierra sources to Central Valley sinks, without substantial channel incision in between (Stock et al., 2005). One possibility is that the uplift is a surface expression of delamination of the lower Sierra Nevada crust (McPhillips and Brandon, 2010), which is also reflected in the Isabella seismic anomaly (Zandt et al., 2004). This is supported by the roughly coincident timing of the delamination and the fast river incision in the early Pleistocene (Stock et al., 2005; Sousa et al., 2017).

Whatever its cause (whether it was dominated by changes in climatic or tectonic forcing or both), once incision on the main-stem canyons commenced, we speculate that the signal of base-level lowering was transmitted upstream along tributaries via knickpoints. However, these knickpoints are presently stalled, a condition that we argue is driven by the observed lack of coarse fluvial sediment to drive bedrock channel incision (Fig. 13). We hypothesize that, when the canyons first began incising rapidly, thick regolith profiles on hillslopes led to long residence times, promoting size reduction due to weathering and thereby reducing the abundance of coarse sediment and thus also the ability of tributaries to keep up with canyon incision. This in turn would have

kept hillslope erosion rates slow and thereby maintained thick weathering profiles and long residence times. Thus, we propose that the signals of base-level lowering on the canyons have been stalled by positive feedbacks between channel incision rate, hillslope erosion rate, regolith residence time, and the abundance of coarse sediment (Fig. 14).

More work is needed to determine whether this feedback sufficiently explains the arrested development in the southern Sierra Nevada and potentially in other landscapes around the world. One possibly fruitful way to test our hypothesis may be to incorporate new findings presented here into a numerical model (e.g., Tucker and Hancock, 2010) that evaluates causes and consequences of the Pleistocene variations in incision rates in the region (e.g., Pelletier 2007). The model would need to account for both tool and cover effects (e.g., Whipple and Tucker, 2002; Sklar and Dietrich, 2006; Johnson, 2014), including particle size efficiency, variations in sediment supply from hillslope erosion, and down-valley fining that results from selective transport and particle wear (Sklar et al., 2017). The new analyses and observations presented here suggest that these factors may be vital components in the strong feedbacks between hillslope weathering, channel incision, and
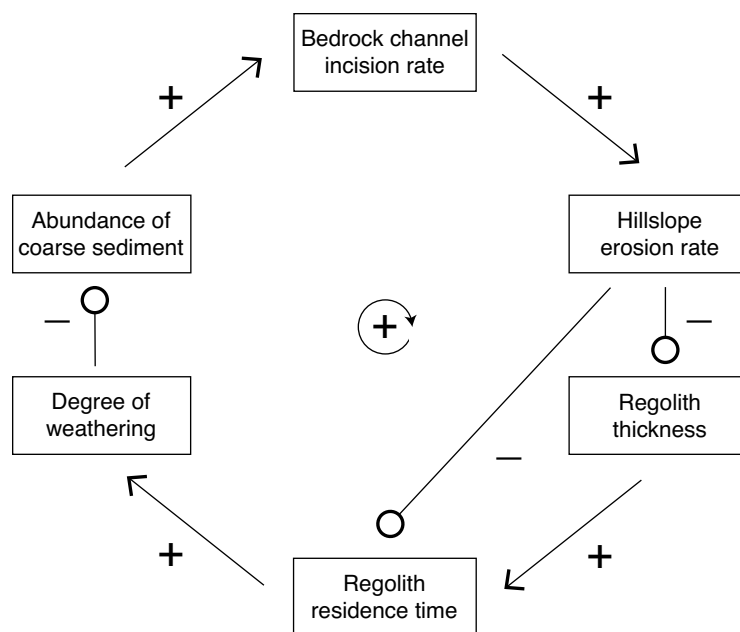
Figure 14. Positive feedbacks between bedrock channel incision rate, hillslope weathering, and sediment size. This illustrates how reductions in river incision rate can be amplified, leading to a slowing of headward migration of risers due to enhanced reduction of sediment size by hillslope weathering. Arrows represent positive couplings, and open symbols represent negative couplings.

landscape response to base-level lowering in the region.

CONCLUSIONS

Tributary creeks and streams draining the western slopes of the southern Sierra Nevada have pronounced knickpoints that separate the landscape into an alternating sequence of gently sloped treads and steeply sloped risers. The presence of the knickpoints and the surrounding "stepped topography" suggest that the landscape is still responding to factor of ~13 changes in incision rates that occurred on main-stem rivers since the early Pleistocene. Contrary to this suggestion, however, cosmogenic nuclide measurements from gently sloped treads and steeply sloped risers show that these features are eroding at similar rates, implying that any headward migration of the knickpoints has largely stalled. In addition, erosion rates of interfluves agree with previously measured canyon incision rates, even though the distribution of knickpoints indicates that the interfluves are relict features adjusted to a previous regional base level. This implies that relief is currently unchanging between the canyons and interfluves, despite the apparent lack of adjustment within the landscape to the Pleistocene changes in incision rates.

The finding of both static knickpoints and static overall interfluve-canyon relief implies that landscape evolution in the southern Sierra Nevada is in a state of arrested development; erosional equilibrium prevails on risers and treads of the region's stepped topography, despite their marked differences in hillslope gradient and despite pronounced Pleistocene canyon cutting along main-stem rivers that drain the range. We propose that this paradox can be explained in part by the region's characteristically thick regolith and moderate erosion rates, which together promote long residence times for regolith on hillslopes. This inhibits survival of coarse sediment during exhumation through the critical zone and thus leads to a paucity of the tools needed for channel incision at bedrock-floored knickpoints. This in turn inhibits headward migration of bedrock knickpoints and has thereby helped preserve interfluves at the drainage divide as relict features of a previous base level. Although we considered several possible explanations for this effect, we hypothesize that the paucity of coarse sediment supply is the primary cause of arrested development in the landscape. Our analysis highlights a feedback in which sediment size reduction due to weathering on hillslopes and transport in channels is both a key response to and regulator of bedrock channel incision and landscape adjustment to base-level changes.

REFERENCES CITED

Aciego, S.M., Riebe, C.S., Hart, S.C., Blakowski, M.A., Carey, C.J., Aarons, S.M., Dove, N.C., Botthoff, J.K., Sims, K.W.W., and Aronson, E.L., 2017, Dust outpaces bedrock in nutrient supply to montane forest ecosystems: Nature Communications, v. 8, p. 14800, https://doi.org/10.1038/ncomms14800.

Arkley, R.J., 1981, Soil moisture use by mixed conifer forest in a summer-dry climate: Soil Science Society of America Journal, v. 45, p. 423–427, https://doi.org/10.2136/sssaj1981.03615995004500020037x.

Arvin, L.J., Riebe, C.S., Aciego, S.M., and Blakowski, M.A., 2017, Global patterns of dust and bedrock nutrient supply to montane ecosystems: Science Advances, v. 3, p. 1588, https://doi.org/10.1126/sciadv.aao1588.

Attal, M., and Lavé, J., 2009, Pebble abrasion during fluvial transport: Experimental results and implications for the evolution of the sediment load along rivers: Journal of Geophysical Research–Earth Surface, v. 114, F04023, https://doi.org/10.1029/2009JF001328.

Attal, M., Mudd, S.M., Hurst, M.D., Weinman, B., Yoo, K., and Naylor, M., 2015, Impact of change in erosion rate and landscape steepness on hillslope and fluvial sediments grain size in the Feather River basin (Sierra Nevada, California): Earth Surface Dynamics, v. 3, p. 201–222, https://doi.org/10.5194/esurf-3-201-2015.

Balco, G., Finnegan, N., Gendaszek, A., Stone, J.O.H., and Thompson, N., 2013, Erosional response to northward-propagating crustal thickening in the coastal ranges of the US Pacific Northwest: American Journal of Science, v. 313, p. 790–806, https://doi.org/10.2475/11.2013.01.

Bales, R.C., Hopmans, J.W., O'Geen, A.T., Meadows, M., Hartsough, P.C., Kirchner, P., Hunsaker, C.T., and Beaudette, D., 2011, Soil moisture response to snowmelt and rainfall in a Sierra Nevada mixed-conifer forest: Vadose Zone Journal, v. 10, p. 786–799, https://doi.org/10.2136/vzj2011.0001.

Bateman, P.C., 1992, Plutonism in the Central Part of the Sierra Nevada Batholith, California: U.S. Geological Survey Professional Paper 1483, 186 p.

Berner, R.A., Lasaga, A.C., and Garrels, R.M., 1983, The carbonate-silicate geochemical cycle and its effect on atmospheric carbon dioxide over the last 100 million years: American Journal of Science, v. 283, p. 641–683, https://doi.org/10.2475/ajs.283.7.641.

Brocard, G.Y., Willenbring, J.K., Miller, T.E., and Scatena, F.N., 2016, Relict landscape resistance to dissection by upstream migrating knickpoints: Journal of Geophysical Research–Earth Surface, v. 121, p. 1182–1203, https://doi.org/10.1002/2015JF003678.

California Department Water Resources, 2013, California Data Exchange Center: http://cdec.water.ca.gov (accessed May, 2017).

Carson, M.A., and Kirkby, M.J., 1972, Hillslope Form and Process: Cambridge, UK, Cambridge University Press, 475 p.

Cassel, E.J., Graham, S.A., and Chamberlain, C.P., 2009, Cenozoic tectonic and topographic evolution of the northern Sierra Nevada, California, through stable isotope paleoaltimetry in volcanic glass: Geology, v. 37, p. 547–550, https://doi.org/10.1130/G25572A.1.

Chabaux, F., Granet, M., Pelt, E., France-Lanord, C., and Galy, V., 2006, ^{238}U-^{234}U-^{230}Th disequilibria and timescale of sedimentary transfers in rivers: Clues from the Gangetic plain rivers: Journal of Geochemical Exploration, v. 88, p. 373–375, https://doi.org/10.1016/j.gexplo.2005.08.078.

Clark, M.K., Maheo, G., Saleeby, J., and Farley, K.A., 2005, The nonequilibrium landscape of the southern Sierra Nevada, California: GSA Today, v. 15, no. 9, p. 4–10, https://doi.org/10.1130/1052-5173(2005)015[4:TNLOTS]2.0.CO;2.

Cook, K.L., Turowski, J.M., and Hovius, N., 2013, A demonstration of the importance of bedload transport for fluvial bedrock erosion and knickpoint propagation: Earth Surface Processes and Landforms, v. 38, p. 683–695, https://doi.org/10.1002/esp.3313.

Cowie, P.A., Whittaker, A.C., Attal, M., Roberts, G., Tucker, G.E., and Ganas, A., 2008, New constraints on sediment-flux–dependent river incision: Implications for extracting tectonic signals from river profiles: Geology, v. 36, p. 535–538, https://doi.org/10.1130/G24681A.1.

Crosby, B.T., and Whipple, K.X., 2006, Knickpoint initiation and distribution within fluvial networks: 236 waterfalls in the Waipaoa River, North Island, New Zealand: Geomorphology, v. 82, p. 16–38, https://doi.org/10.1016/j.geomorph.2005.08.023.

Crosby, B.T., Whipple, K.X., Gasparini, N.M., and Wobus, C.W., 2007, Formation of fluvial hanging valleys: Theory and simulation: Journal of Geophysical Research–Earth Surface, v. 112, F03S10, https://doi.org/10.1029/2006JF000566.

Cyr, A.J., and Granger, D.E., 2008, Dynamic equilibrium among erosion, river incision, and coastal uplift in the Northern and Central Apennines, Italy: Geology, v. 36, p. 103–106, https://doi.org/10.1130/G24003A.1.

Cyr, A.J., Granger, D.E., Olivetti, V., and Molin, P., 2010, Quantifying rock uplift rates using channel steepness and cosmogenic nuclide–determined erosion rates: Examples from northern and southern Italy: Lithosphere, v. 2, p. 188–198, https://doi.org/10.1130/L96.1.

Dahlgren, R.A., Boettinger, J.L., Huntington, G.L., and Amundson, R.G., 1997, Soil development along an elevational transect in the western Sierra Nevada, California: Geoderma, v. 78, p. 207–236, https://doi.org/10.1016/S0016-7061(97)00034-7.

Dequincey, O., Chabaux, F., Clauer, N., Sigmarsson, O., Liewig, N., and Leprun, J.C., 2002, Chemical mobilizations in laterites; evidence from trace elements and ^{238}U-^{234}U-^{230}Th disequilibria: Geochimica et Cosmochimica Acta, v. 66, no. 7, p. 1197–1210, https://doi.org/10.1016/S0016-7037(01)00845-6.

DiBiase, R.A., Heimsath, A.M., and Whipple, K.X., 2012, Hillslope response to tectonic forcing in threshold landscapes: Earth Surface Processes and Landforms, v. 37, p. 855–865, https://doi.org/10.1002/esp.3205.

DiBiase, R.A., Whipple, K.X., Lamb, M.P., and Heimsath, A.M., 2015, The role of waterfalls and knickzones in controlling the style and pace of landscape adjustment in the western San Gabriel Mountains, California: Geological Society of America Bulletin, v. 127, p. 539–559, https://doi.org/10.1130/B31113.1.

DiBiase, R.A., Rossi, M.W., and Neely, A.B., 2018, Fracture density and grain size controls on the relief structure of bedrock landscapes: Geology, v. 46, p. 399–402, https://doi.org/10.1130/G40006.1.

Ditchburn, R.G., and Whitehead, N.E., 1994, The separation of ^{10}Be from silicates, *in* Proceedings of the 3rd Workshop of the South Pacific Environmental Radioactivity Association: Canberra, Australia, South Pacific Environmental Radioactivity Association, p. 4–7.

Dixon, J.L., 2008, Landscape Response to Climate Forcing: Quantifying Mechanisms and Rates of Erosion and Weathering along an Orographically Enhanced Climate Gradient [Ph.D. thesis]: Hanover, New Hampshire, Dartmouth College, 174 p.

Dixon, J.L., and Riebe, C.S., 2014, Tracing and pacing soil across slopes: Elements, v. 10, p. 363–368, https://doi.org/10.2113/gselements.10.5.363.

Dixon, J.L., Heimsath, A.M., and Amundson, R., 2009a, The critical role of climate and saprolite weathering in landscape evolution: Earth Surface Processes and Landforms, v. 34, p. 1507–1521, https://doi.org/10.1002/esp.1836.

Dixon, J.L., Heimsath, A.M., Kaste, J., and Amundson, R., 2009b, Climate-driven processes of hillslope weathering: Geology, v. 37, p. 975–978, https://doi.org/10.1130/G30045A.1.

Dosseto, A., and Schaller, M., 2016, The erosion response to Quaternary climate change quantified using uranium isotopes and in situ–produced cosmogenic nuclides: Earth-Science Reviews, v. 155, p. 60–81, https://doi.org/10.1016/j.earscirev.2016.01.015.

Dosseto, A., Bourdon, B., and Turner, S.P., 2008a, Uranium-series isotopes in river materials: Insights into the timescales of erosion and sediment transport: Earth and Planetary Science Letters, v. 265, p. 1–17, https://doi.org/10.1016/j.epsl.2007.10.023.

Dosseto, A., Turner, S.P., and Chappell, J., 2008b, The evolution of weathering profiles through time: New insights from uranium-series isotopes: Earth and Planetary Science Letters, v. 274, p. 359–371, https://doi.org/10.1016/j.epsl.2008.07.050.

Dosseto, A., Hesse, P.P., Maher, K., Fryirs, K., and Turner, S., 2010, Climatic and vegetation control on sediment dynamics during the last glacial cycle: Geology, v. 38, p. 395–398, https://doi.org/10.1130/G30708.1.

Dosseto, A., Buss, H.L., and Chabaux, F., 2014, Age and weathering rate of sediments in small catchments: The role of hillslope erosion: Geochimica et Cosmochimica Acta, v. 132, p. 238–258, https://doi.org/10.1016/j.gca.2014.02.010.

Egholm, D.L., Knudsen, M.F., and Sandiford, M., 2013, Lifespan of mountain ranges scaled by feedbacks between landsliding and erosion by rivers: Nature, v. 498, p. 475–478, https://doi.org/10.1038/nature12218.

Ferrier, K.L., Huppert, K.L., and Perron, J.T., 2013, Climatic control of bedrock river incision: Nature, v. 496, p. 206–209, https://doi.org/10.1038/nature11982.

Ferrier, K.L., Riebe, C.S., and Hahm, W.J., 2016, Testing for supply-limited and kinetic-limited chemical erosion in field measurements of regolith production and chemical depletion: Geochemistry Geophysics Geosystems, v. 17, p. 2270–2285, https://doi.org/10.1002/2016GC006273.

Flinchum, B.A., Steven Holbrook, W., Rempe, D., Moon, S., Riebe, C.S., Carr, B.J., Hayes, J.L., St. Clair, J., and Peters, M.P., 2018, Critical zone structure under a granite ridge inferred from drilling and three-dimensional seismic refraction data: Journal of Geophysical Research, Earth Surface, v. 123, p. 1317–1343, https://doi.org/10.1029/2017JF004280.

Gabet, E.J., 2014, Late Cenozoic uplift of the Sierra Nevada, California? A critical analysis of the geomorphic evidence: American Journal of Science, v. 314, p. 1224–1257, https://doi.org/10.2475/08.2014.03.

Gilbert, G.K., 1877, Report on the Geology of the Henry Mountains (Utah): Washington, D.C., U.S. Geographical and Geological Survey, Publication of the Powell Survey, Government Printing Office, 160 p.

Gillespie, A.R., and Zehfuss, P.H., 2004, Glaciations of the Sierra Nevada, California, USA, in Ehlers, J., and Gibbard, P.L., eds., Quaternary Glaciations—Extent and Chronology. Part II: North America: Amsterdam, The Netherlands, Elsevier, Developments in Quaternary Sciences Volume 2, p. 51–62.

Goodfellow, B.W., Hilley, G.E., Webb, S.M., Sklar, L.S., Moon, S., and Olson, C.A., 2016, The chemical, mechanical, and hydrological evolution of weathering granitoid: Journal of Geophysical Research–Earth Surface, v. 121, p. 1410–1435, https://doi.org/10.1002/2016JF003822.

Goulden, M.L., and Bales, R.C., 2014, Mountain runoff vulnerability to increased evapotranspiration with vegetation expansion: Proceedings of the National Academy of Sciences of the United States of America, v. 111, no. 39, p. 14,071–14,075, https://doi.org/10.1073/pnas.1319316111.

Goulden, M.L., Anderson, R.G., Bales, R.C., Kelly, A.E., Meadows, M., and Winston, G.C., 2012, Evapotranspiration along an elevation gradient in California's Sierra Nevada: Journal of Geophysical Research–Earth Surface, v. 117, G03028, https://doi.org/10.1029/2012JG002027.

Graham, R.C., Rossi, A.M., and Hubbert, K.R., 2010, Rock to regolith conversion: Producing hospitable substrates for terrestrial ecosystems: GSA Today, v. 20, no. 2, p. 4–9, https://doi.org/10.1130/GSAT57A.1.

Granet, M., Chabaux, F., Stille, P., Dosseto, A., France-Lanord, C., and Blaes, E., 2010, U-series disequilibria in suspended river sediments and implication for sediment transfer time in alluvial plains: The case of the Himalayan rivers: Geochimica et Cosmochimica Acta, v. 74, p. 2851–2865, https://doi.org/10.1016/j.gca.2010.02.016.

Granger, D.E., and Riebe, C.S., 2014, Cosmogenic nuclides in weathering and erosion, in Drever, J.I., ed., Treatise on Geochemistry, Volume 5: Surface and Ground Water, Weathering, and Soils. (2nd ed.): Oxford, UK, Elsevier Ltd., p. 401–436, https://doi.org/10.1016/B978-0-08-095975-7.00514-3.

Granger, D.E., and Smith, A.L., 2000, Dating buried sediments using radioactive decay and muogenic production of ^{26}Al and ^{10}Be: Nuclear Instruments & Methods in Physics Research, Section B, Beam Interactions with Materials and Atoms, v. 172, p. 822–826, https://doi.org/10.1016/S0168-583X(00)00087-2.

Granger, D.E., Kirchner, J.W., and Finkel, R., 1996, Spatially averaged long-term erosion rates measured from in-situ produced cosmogenic nuclides in alluvial sediment: The Journal of Geology, v. 104, p. 249–257, https://doi.org/10.1086/629823.

Granger, D.E., Riebe, C.S., Kirchner, J.W., and Finkel, R.C., 2001, Modulation of erosion on steep granitic slopes by boulder armoring, as revealed by cosmogenic ^{26}Al and ^{10}Be: Earth and Planetary Science Letters, v. 186, p. 269–281, https://doi.org/10.1016/S0012-821X(01)00236-9.

Hahm, W.J., Riebe, C.S., Lukens, C.E., and Araki, S., 2014, Bedrock composition regulates mountain ecosystems and landscape evolution: Proceedings of the National Academy of Sciences of the United States of America, v. 111, no. 9, p. 3338–3343, https://doi.org/10.1073/pnas.1315667111.

Hake, B.F., 1928, Scarps of the southwestern Sierra Nevada, California: Geological Society of America Bulletin, v. 39, p. 1017–1030, https://doi.org/10.1130/GSAB-39-1017.

Hammond, W.C., Blewitt, G., and Kreemer, C., 2016, GPS imaging of vertical land motion in California and Nevada: Implications for Sierra Nevada uplift: Journal of Geophysical Research–Solid Earth, v. 121, p. 7681–7703, https://doi.org/10.1002/2016JB013458.

Hancock, G.S., and Anderson, R.S., 2002, Numerical modelling of fluvial strath terrace formation in response to oscillating climate: Geological Society of America Bulletin, v. 114, p. 1131–1142, https://doi.org/10.1130/0016-7606(2002)114<1131.

Heller, P.L., Beland, P.E., Humphrey, N.F., Konrad, S.K., Lynds, R.M., McMillan, M.E., Valentine, K.E., Widman, Y.A., and Furbish, D.J., 2001, Paradox of downstream fining and weathering-rind formation in the lower Hoh River, Olympic Peninsula, Washington: Geology, v. 29, p. 971–974, https://doi.org/10.1130/0091-7613(2001)029<0971:PODFAW>2.0.CO;2.

Holbrook, W.S., Riebe, C.S., Elwaseif, M., Hayes, J.L., Basler Reeder, K., Harry, D.L., Malazian, A., Dosseto, A., Hartsough, P.C., and Hopmans, J.W., 2014, Geophysical constraints on deep weathering and water storage potential in the Southern Sierra Critical Zone Observatory: Earth Surface Processes and Landforms, v. 39, p. 366–380, https://doi.org/10.1002/esp.3502.

House, M., Wernicke, B., Farley, K., and Dumitru, T., 1997, Cenozoic thermal evolution of the central Sierra Nevada, California, from (U-Th)/He thermochronometry: Earth and Planetary Science Letters, v. 151, p. 167–179, https://doi.org/10.1016/S0012-821X(97)81846-8.

House, M.A., Wernicke, B.P., and Farley, K.A., 1998, Dating topography of the Sierra Nevada, California, using apatite (U-Th)/He ages: Nature, v. 396, p. 66–69, https://doi.org/10.1038/23926.

Huber, N.K., 1981, Amount and Timing of Late Cenozoic Uplift and Tilt of the Central Sierra Nevada, California— Evidence from the Upper San Joaquin River Basin: U.S. Geological Survey Professional Paper 1197, 28 p.

Hunsaker, C.T., and Neary, D.G., 2012, Sediment loads and erosion in forest headwater streams of the Sierra Nevada, California, in Webb, A.A., et al., eds., Revisiting Experimental Catchment Studies in Forest Hydrology: International Association of Hydrological Sciences Publication 353, p. 195–203.

Hurst, M.D., Mudd, S.M., Walcott, R., Attal, M., and Yoo, K., 2012, Using hilltop curvature to derive the spatial distribution of erosion rates: Journal of Geophysical Research–Earth Surface, v. 117, p. F02017, https://doi.org/10.1029/2011JF002057.

Hurst, M.D., Mudd, S.M., Yoo, K., Attal, M., and Walcott, R., 2013, Influence of lithology on hillslope morphology and response to tectonic forcing in the northern Sierra Nevada of California: Journal of Geophysical Research–Earth Surface, v. 118, p. 832–851, https://doi.org/10.1002/jgrf.20049.

Jenny, H., Gessel, S.P., and Bingham, F.T., 1949, Comparative study of decomposition rates of organic matter in temperate and tropical regions: Soil Science, v. 68, p. 419–432, https://doi.org/10.1097/00010694-194912000-00001.

Jessup, B.S., Hahm, W.J., Miller, S.N., Kirchner, J.W., and Riebe, C.S., 2011, Landscape response to tipping points in granite weathering: The case of stepped topography in the Southern Sierra Critical Zone Observatory: Applied Geochemistry, v. 26, supplement, p. S48–S50, https://doi.org/10.1016/j.apgeochem.2011.03.026.

Johnson, D.W., Hunsaker, C.T., Glass, D.W., Rau, B.M., and Roath, B.A., 2011, Carbon and nutrient contents in soils from the Kings River Experimental Watersheds, Sierra Nevada Mountains, California: Geoderma, v. 160, p. 490–502, https://doi.org/10.1016/j.geoderma.2010.10.019.

Johnson, J.P.L., 2014, A surface roughness model for predicting alluvial cover and bed load transport rate in bedrock channels: Journal of Geophysical Research–Earth Surface, v. 119, p. 2147–2173, https://doi.org/10.1002/2013JF003000.

Kellndorfer, J., Walker, W., Kirsch, K., Fiske, G., Bishop, J., LaPoint, L., Hoppus, M., and Westfall, J., 2013, NACP Aboveground Biomass and Carbon Baseline Data (NBCD 2000), USA, 2000 (ORNLDAAC): https://daac.ornl.gov/NACP/guides/NBCD_2000_V2.html (accessed May, 2017), http://dx.doi.org/10.3334/ORNLDAAC/1081.

Kigoshi, K., 1971, Alpha-recoil thorium-234: Dissolution into water and the uranium-234/uranium-238 disequilibrium in nature: Science, v. 173, p. 47–48, https://doi.org/10.1126/science.173.3991.47.

Klos, P.Z., Goulden, M., Riebe, C., Tague, C., O'Green, A.T., Flinchum, B., Safeeq, M., Conklin, M., Hart, S., Berhe, A.A., Hartsough, P., Holbrook, W.S., and Bales, R., 2018, Predicting plant-accessible water in the critical zone: Mountain ecosystems in a Mediterranean climate: WIREs Water, v. 5, no. 3, p. e1277, https://doi.org/10.1002/wat2.1277.

Kohl, C.P., and Nishiizumi, K., 1992, Chemical isolation of quartz for measurement of in-situ–produced cosmogenic nuclides: Geochimica et Cosmochimica Acta, v. 56, p. 3583–3587, https://doi.org/10.1016/0016-7037(92)90401-4.

Krugh, W.C., and Foreshee, B.C., 2018, Geomorphic constraints on the incision history of the lower Kern River, southern Sierra Nevada, California: Geosphere, v. 14, p. 1101–1118, https://doi.org/10.1130/GES01603.1.

Lackey, J.S., Cecil, M.R., Windham, C.J., Frazer, R.E., Bindeman, I.N., and Gehrels, G.E., 2012, The Fine Gold intrusive suite: The roles of basement terranes and magma source development in the Early Cretaceous Sierra Nevada batholith: Geosphere, v. 8, p. 292–313, https://doi.org/10.1130/GES00745.1.

Lamb, M.P., Dietrich, W.E., and Sklar, L.S., 2008, A model for fluvial bedrock incision by impacting suspended and bed load sediment: Journal of Geophysical Research–Earth Surface, v. 113, F03025, https://doi.org/10.1029/2007JF000915.

Larsen, I.J., Montgomery, D.R., and Greenberg, H.M., 2014, The contribution of mountains to global denudation: Geology, v. 42, p. 527–530, https://doi.org/10.1130/G35136.1.

Lindgren, W., 1911, The Tertiary Gravels of the Sierra Nevada of California: U.S. Geological Survey Professional Paper 79, 73 p., https://doi.org/10.3133/pp73.

Lukens, C.E., 2016, Spatial Variation in Sediment Production Across Mountain Catchments: Insights from Cosmogenic Nuclides and Tracer Thermochronometry [Ph.D. thesis]: Laramie, Wyoming, University of Wyoming, 178 p.

Lukens, C.E., Riebe, C.S., Sklar, L.S., and Shuster, D.L., 2016, Grain size bias in cosmogenic nuclide studies of stream sediment in steep terrain: Journal of Geophysical Research–Earth Surface, v. 121, p. 978–999, https://doi.org/10.1002/2016JF003859.

Luo, X., Rehkämper, M., Lee, D.-C., and Halliday, A.N., 1997, High precision ^{230}Th/^{232}Th and ^{234}U/^{238}U measurements using energy filtered ICP magnetic sector multiple collector mass spectrometry: International Journal of Mass Spectrometry and Ion Processes, v. 171, p. 105–117, https://doi.org/10.1016/S0168-1176(97)00136-5.

Madoff, R.D., and Putkonen, J., 2016, Climate and hillslope degradation vary in concert; 85 ka to present, eastern Sierra Nevada, CA, USA: Geomorphology, v. 266, p. 33–40, https://doi.org/10.1016/j.geomorph.2016.05.010.

Maher, K., and Chamberlain, C.P., 2014, Hydrologic regulation of chemical weathering and the geologic carbon cycle: Science, v. 343, p. 1502–1504, https://doi.org/10.1126/science.1250770.

Marshall, J.A., and Sklar, L.S., 2012, Mining soil databases for landscape-scale patterns in the abundance and size distribution of hillslope rock fragments: Earth Surface Processes and Landforms, v. 37, p. 287–300, https://doi.org/10.1002/esp.2241.

Marshall, J.A., Roering, J.J., Bartlein, P.J., Gavin, D.G., Granger, D.E., Rempel, A.W., Praskievicz, S.J., and Hales, T.C., 2015, Frost for the trees: Did climate increase erosion in unglaciated landscapes during the late Pleistocene?: Science Advances, v. 1, no. 10, p. e1500715, https://doi.org/10.1126/sciadv.1500715.

Marshall, J.A., Roering, J.J., Gavin, D.G., and Granger, D.E., 2017, Late Quaternary climatic controls on erosion rates and geomorphic processes in western Oregon, USA: Geological Society of America Bulletin, v. 129, p. 715–731, https://doi.org/10.1130/B31509.1.

Martin, A.N., Dosseto, A., and Kinsley, L.P.J., 2015, Evaluating the removal of non-detrital matter from soils and sediment using uranium isotopes: Chemical Geology, v. 396, p. 124–133, https://doi.org/10.1016/j.chemgeo.2014.12.016.

Matthes, F.E., 1960, Reconnaissance of the Geomorphology and Glacial Geology of the San Joaquin Basin, Sierra Nevada, California: U.S. Geological Survey Professional Paper 329, 62 p., https://doi.org/10.3133/pp329.

McPhillips, D., and Brandon, M.T., 2010, Using tracer thermochronology to measure modern relief change in the Sierra Nevada, California: Earth and Planetary Science Letters, v. 296, p. 373–383, https://doi.org/j.epsl.2010.05.022.

McPhillips, D., and Brandon, M.T., 2012, Topographic evolution of the Sierra Nevada measured directly by inversion of low-temperature thermochronology: American Journal of Science, v. 312, p. 90–116, https://doi.org/10.2475/02.2012.02.

Miller, J.R., 1991, The influence of bedrock geology on knickpoint development and channel-bed degradation along downcutting streams in south-central Indiana: The Journal of Geology, v. 99, p. 591–605, https://doi.org/10.1086/629519.

Miller, K.L., Szabó, T., Jerolmack, D.J., and Domokos, G., 2014, Quantifying the significance of abrasion and selective transport for downstream fluvial grain size evolution: Journal of Geophysical Research–Earth Surface, v. 119, p. 2412–2429, https://doi.org/10.1002/2014JF003156.

Mudd, S.M., Harel, M.-A., Hurst, M.D., Grieve, S.W.D., and Marrero, S.M., 2016, The CAIRN method: Automated, reproducible calculation of catchment-averaged denudation rates from cosmogenic nuclide concentrations: Earth Surface Dynamics, v. 4, p. 655–674, https://doi.org/10.5194/esurf-4-655-2016.

Mulch, A., Graham, S.A., and Chamberlain, C.P., 2006, Hydrogen isotopes in Eocene river gravels and paleoelevation of the Sierra Nevada: Science, v. 313, p. 87–89, https://doi.org/10.1126/science.1125986.

Murphy, B.P., Johnson, J.P.L., Gasparini, N.M., and Sklar, L.S., 2016, Chemical weathering as a mechanism for the climatic control of bedrock river incision: Nature, v. 532, p. 223–227, https://doi.org/10.1038/nature17449.

Muzikar, P., Elmore, D., and Granger, D.E., 2003, Accelerator mass spectrometry in geologic research: Geological Society of America Bulletin, v. 115, p. 643–654, https://doi.org/10.1130/0016-7606(2003)115<0643:AMSIGR>2.0.CO;2.

Panzer, V.W., 1933, Die kalifornische Sierra Nevada als Rumpftreppe: Geologische Rundschau, v. 33, p. 201–205.

Paola, C., Parker, G., Seal, R., Sinha, S.K., Southard, J.B., and Wilcock, P.R., 1992, Downstream fining by selective deposition in a laboratory flume: Science, v. 258, p. 1757–1760, https://doi.org/10.1126/science.258.5089.1757.

Parameter-Elevation Regressions on Independent Slopes Model (PRISM) Climate Group, 2017, Parameter-Elevation Regressions on Independent Slopes Model (PRISM): PRISM Climate Group, Oregon State University, http://prism.oregonstate.edu (created 9 May 2017).

Pelletier, J.D., 2007, Numerical modeling of the Cenozoic geomorphic evolution of the southern Sierra Nevada, California: Earth and Planetary Science Letters, v. 259, p. 85–96, https://doi.org/10.1016/j.epsl.2007.04.030.

Penck, W., 1924, Morphological Analysis of Land Forms: A Contribution to Physical Geology (translated by H. Czech and K.C. Boswell): London, MacMillan and Co. Ltd., republished 1953, 429 p.

Portenga, E.W., and Bierman, P.R., 2011, Understanding Earth's eroding surface with ^{10}Be: GSA Today, v. 21, no. 8, p. 4–10, https://doi.org/10.1130/G111A.1.

PRIME Lab, 2013, Mineral Separation Procedure: http://www.physics.purdue.edu/primelab/labs/mineral-separation-lab/procedure.php (July 2013).

Raymo, M.E., Ruddiman, W.F., and Froelich, P.N., 1988, Influence of late Cenozoic mountain building on ocean geochemical cycles: Geology, v. 16, p. 649–653, https://doi.org/10.1130/0091-7613(1988)016<0649:IOLCMB>2.3.CO;2.

Riebe, C.S., and Granger, D.E., 2013, Quantifying effects of deep and near-surface chemical erosion on cosmogenic nuclides in soils, saprolite, and sediment: Earth Surface Processes and Landforms, v. 38, p. 523–533, https://doi.org/10.1002/esp.3339.

Riebe, C.S., Kirchner, J.W., Granger, D.E., and Finkel, R.C., 2000, Erosional equilibrium and disequilibrium in the Sierra Nevada, inferred from cosmogenic ^{26}Al and ^{10}Be in alluvial sediment: Geology, v. 28, p. 803–806, https://doi.org/10.1130/0091-7613(2000)28<803:EEADIT>2.0.CO;2.

Riebe, C.S., Kirchner, J.W., Granger, D.E., and Finkel, R.C., 2001a, Minimal climatic control on erosion rates in the Sierra Nevada, California: Geology, v. 29, p. 447–450, https://doi.org/10.1130/0091-7613(2001)029<0447:MCCOER>2.0.CO;2.

Riebe, C.S., Kirchner, J.W., Granger, D.E., and Finkel, R.C., 2001b, Strong tectonic and weak climatic control of long-term chemical weathering rates: Geology, v. 29, p. 511–514, https://doi.org/10.1130/0091-7613(2001)029<0511:STAWCC>2STAWCC>2.0.CO;2.

Riebe, C.S., Kirchner, J.W., and Finkel, R.C., 2004, Erosional and climatic effects on long-term chemical weathering rates in granitic landscapes spanning diverse climate regimes: Earth and Planetary Science Letters, v. 224, p. 547–562, https://doi.org/10.1016/j.epsl.2004.05.019.

Riebe, C.S., Sklar, L.S., Lukens, C.E., and Shuster, D.L., 2015, Climate and topography control the size and flux of sediment produced on steep mountain slopes: Proceedings of the National Academy of Sciences of the United States of America, v. 112, p. 15,574–15,579, https://doi.org/10.1073/pnas.1503567112.

Riebe, C.S., Hahm, W.J., and Brantley, S.L., 2017, Controls on deep critical zone architecture: A historical review and four testable hypotheses: Earth Surface Processes and Landforms, v. 42, p. 128–156, https://doi.org/10.1002/esp.4052.

Rood, D.H., Hall, S., Guilderson, T.P., Finkel, R.C., and Brown, T.A., 2010, Challenges and opportunities in high-precision Be-10 measurements at CAMS: Nuclear Instruments & Methods in Physics Research, Section B, Beam Interactions with Materials and Atoms, v. 268, p. 730–732, https://doi.org/10.1016/j.nimb.2009.10.016.

Saleeby, J., Ducea, M., and Clemens-Knott, D., 2003, Production and loss of high-density batholithic root, southern Sierra Nevada, California: Tectonics, v. 22, 1064, https://doi.org/10.1029/2002TC001374.

Schachtman, N.S., Roering, J.J., Marshall, J.A., Gavin, D.G., and Granger, D.E., 2016, Using a paleo perspective to demonstrate climate controls on glacial-interglacial weathering: Insights from Little Lake, OR: San Francisco, California, American Geophysical Union, 2016 Fall Meeting, abstract EP33B-0982.

Scheingross, J.S., and Lamb, M.P., 2016, Sediment transport through self-adjusting, bedrock-walled waterfall plunge pools: Journal of Geophysical Research–Earth Surface, v. 121, p. 939–963, https://doi.org/10.1002/2015JF003620.

Shobe, C.M., Tucker, G.E., and Anderson, R.S., 2016, Hillslope-derived blocks retard river incision: Geophysical Research Letters, v. 43, p. 5070–5078, https://doi.org/10.1002/2016GL069262.

Shuster, D.L., Ehlers, T.A., Rusmore, M.E., and Farley, K.A., 2005, Rapid glacial erosion at 1.8 Ma revealed by ^{4}He/^{3}He thermochronometry: Science, v. 310, p. 1668–1670, https://doi.org/10.1126/science.1118519.

Sklar, L.S., and Dietrich, W.E., 1998, River longitudinal profiles and bedrock incision models: Stream power and the influence of sediment supply, *in* Tinkler, K.J., and Wohl, E.E., eds., Rivers over Rock: Fluvial Processes in Bedrock Channels: American Geophysical Union Geophysical Monograph 107, p. 237–260, https://doi.org/10.1029/GM107p0237.

Sklar, L.S., and Dietrich, W.E., 2001, Sediment and rock strength controls on river incision into bedrock: Geology, v. 29, no. 12, p. 1087–1090, https://doi.org/10.1130/0091-7613(2001)029<1087:SARSCO>2.0.CO;2.

Sklar, L.S., and Dietrich, W.E., 2004, A mechanistic model for river incision into bedrock by saltating bed load: Water Resources Research, v. 40, W06301, https://doi.org/10.1029/2003WR002496.

Sklar, L.S., and Dietrich, W.E., 2006, The role of sediment in controlling steady-state bedrock channel slope: Implications of the saltation-abrasion incision model: Geomorphology, v. 82, p. 58–83, https://doi.org/10.1016/j.geomorph.2005.08.019.

Sklar, L.S., Dietrich, W.E., Foufoula-Georgiou, E., Lashermes, B., and Bellugi, D., 2006, Do gravel bed river size distributions record channel network structure?: Water Resources Research, v. 42, W06D18, https://doi.org/10.1029/2006WR005035.

Sklar, L.S., Riebe, C.S., Lukens, C.E., and Bellugi, D., 2016, Catchment power and the joint distribution of elevation and travel distance to the outlet: Earth Surface Dynamics, v. 4, p. 799–818, https://doi.org/10.5194/esurf-4-799-2016.

Sklar, L.S., Riebe, C.S., Marshall, J.A., Genetti, J., Leclere, S., Lukens, C.L., and Merces, V., 2017, The problem of predicting the size distribution of sediment supplied by hillslopes to rivers: Geomorphology, v. 277, p. 31–49, https://doi.org/10.1016/j.geomorph.2016.05.005.

Small, E.E., and Anderson, R.S., 1995, Geomorphically driven late Cenozoic rock uplift in the Sierra Nevada, California: Science, v. 270, p. 277–281, https://doi.org/10.1126/science.270.5234.277.

Small, E.E., Anderson, R.S., Repka, J.L., and Finkel, R.C., 1997, Erosion rates of alpine bedrock summit surfaces deduced from in situ ^{10}Be and ^{26}Al: Earth and Planetary Science Letters, v. 150, p. 413–425, https://doi.org/10.1016/S0012-821X(97)00092-7.

Sosa Gonzalez, V., Schmidt, A.H., Bierman, P.R., and Rood, D.H., 2017, Spatial and temporal replicability of meteoric and in situ ^{10}Be concentrations in fluvial sediment: Earth Surface Processes and Landforms, v. 42, p. 2570–2584, https://doi.org/10.1002/esp.4205.

Sousa, F.J., Farley, K.A., Saleeby, J., and Clark, M., 2016, Eocene activity on the Western Sierra fault system and its role incising Kings Canyon, California: Earth and

Planetary Science Letters, v. 439, p. 29–38, https://doi.org/10.1016/j.epsl.2016.01.020.

Sousa, F.J., Saleeby, J., Farley, K.A., Unruh, J.R., and Lloyd, M.K., 2017, The southern Sierra Nevada pediment, central California: Geosphere, v. 13, p. 82–101, https://doi.org/10.1130/GES01369.1.

Springer, G.S., Tooth, S., and Wohl, E.E., 2005, Dynamics of pothole growth as defined by field data and geometrical description: Journal of Geophysical Research–Earth Surface, v. 110, F04010, https://doi.org/10.1029/2005JF000321.

Stock, G.M., Anderson, R.S., and Finkel, R.C., 2004, Pace of landscape evolution in the Sierra Nevada, California, revealed by cosmogenic dating of cave sediments: Geology, v. 32, p. 193–196, https://doi.org/10.1130/G20197.1.

Stock, G.M., Anderson, R.S., and Finkel, R.C., 2005, Rates of erosion and topographic evolution of the Sierra Nevada, California, inferred from cosmogenic ^{26}Al and ^{10}Be concentrations: Earth Surface Processes and Landforms, v. 30, p. 985–1006, https://doi.org/10.1002/esp.1258.

Stock, G.M., Ehlers, T.A., and Farley, K.A., 2006, Where does sediment come from? Quantifying catchment erosion with detrital apatite (U-Th)/He thermochronometry: Geology, v. 34, p. 725–728, https://doi.org/10.1130/G22592.1.

Tucker, G.E., and Hancock, G.R., 2010, Modelling landscape evolution: Earth Surface Processes and Landforms, v. 35, p. 28–50, https://doi.org/10.1002/esp.1952.

Turowski, J.M., Wyss, C.R., and Beer, A.R., 2015, Grain size effects on energy delivery to the streambed and links to bedrock erosion: Geophysical Research Letters, v. 42, p. 1775–1780, https://doi.org/10.1002/2015GL063159.

Unruh, J.R., 1991, The uplift of the Sierra Nevada and implications for late Cenozoic epeirogeny in the western Cordillera: Geological Society of America Bulletin, v. 103, p. 1395–1404, https://doi.org/10.1130/0016-7606(1991)103<1395:TUOTSN>2.0.CO;2.

U.S. Geological Survey, 2009, National Agricultural Imagery Program: https://lta.cr.usgs.gov/NAIP/ (accessed September, 2009).

Wahrhaftig, C., 1965, Stepped topography of the southern Sierra Nevada, California: Geological Society of America Bulletin, v. 76, p. 1165–1190, https://doi.org/10.1130/0016-7606(1965)76[1165:STOTSS]2.0.CO;2.

Wakabayashi, J., 2013, Paleochannels, stream incision, erosion, topographic evolution, and alternative explanations of paleoaltimetry, Sierra Nevada, California: Geosphere, v. 9, p. 191–215, https://doi.org/10.1130/GES00814.1.

Wakabayashi, J., and Sawyer, T.L., 2001, Stream incision, tectonics, uplift, and evolution of topography of the Sierra Nevada, California: The Journal of Geology, v. 109, p. 539–562, https://doi.org/10.1086/321962.

Walker, J.C.G., Hays, P.B., and Kasting, J.F., 1981, A negative feedback mechanism for the long-term stabilization of Earth's surface temperature: Journal of Geophysical Research, v. 86, p. 9776–9782, https://doi.org/10.1029/JC086iC10p09776.

Wheeler, L.B., Galewsky, J., Herold, N., and Huber, M., 2016, Late Cenozoic surface uplift of the southern Sierra Nevada (California, USA): A paleoclimate perspective on lee-side stable isotope paleoaltimetry: Geology, v. 44, p. 451–454, https://doi.org/10.1130/G37718.1.

Whipple, K.X., 2004, Bedrock rivers and the geomorphology of active orogens: Annual Review of Earth and Planetary Sciences, v. 32, p. 151–185, https://doi.org/10.1146/annurev.earth.32.101802.120356.

Whipple, K.X., and Tucker, G.E., 1999, Dynamics of the stream-power river incision model: Implications for height limits of mountain ranges, landscape response timescales, and research needs: Journal of Geophysical Research–Solid Earth, v. 104, p. 17,661–17,674, https://doi.org/10.1029/1999JB900120.

Whipple, K.X., and Tucker, G.E., 2002, Implications of sediment-flux–dependent river incision models for landscape evolution: Journal of Geophysical Research–Solid Earth, v. 107, 2039, https://doi.org/10.1029/2000JB000044.

Whipple, K.X., Hancock, G.S., and Anderson, R.S., 2000, River incision into bedrock: Mechanics and relative efficacy of plucking, abrasion, and cavitation: Geological Society of America Bulletin, v. 112, p. 490–503, https://doi.org/10.1130/0016-7606(2000)112<490:RIIBMA>2.0.CO;2.

Whittaker, A.C., Cowie, P.A., Attal, M., Tucker, G.E., and Roberts, G.P., 2007, Bedrock channel adjustment to tectonic forcing: Implications for predicting river incision rates: Geology, v. 35, p. 103–106, https://doi.org/10.1130/G23106A.1.

Willenbring, J.K., Codilean, A.T., and McElroy, B., 2013a, Earth is (mostly) flat: Apportionment of the flux of continental sediment over millennial time scales: Geology, v. 41, p. 343–346, https://doi.org/10.1130/G33918.1.

Willenbring, J.K., Gasparini, N.M., Crosby, B.T., and Brocard, G., 2013b, What does a mean mean? The temporal evolution of detrital cosmogenic denudation rates in a transient landscape: Geology, v. 41, p. 1215–1218, https://doi.org/10.1130/G34746.1.

Wobus, C.W., Crosby, B.T., and Whipple, K.X., 2006, Hanging valleys in fluvial systems: Controls on occurrence and implications for landscape evolution: Journal of Geophysical Research–Earth Surface, v. 111, F02017, https://doi.org/10.1029/2005JF000406.

Wohl, E.E., Thompson, D.M., and Miller, A.J., 1999, Canyons with undulating walls: Geological Society of America Bulletin, v. 111, p. 949–959, https://doi.org/10.1130/0016-7606(1999)111<0949:CWUW>2.3.CO;2.

Woolfenden, W.B., 2003, A 180,000-year pollen record from Owens Lake, CA: Terrestrial vegetation change on orbital sales: Quaternary Research, v. 59, p. 430–444, https://doi.org/10.1016/S0033-5894(03)00033-4.

Yoo, K., and Mudd, S.M., 2008, Discrepancy between mineral residence time and soil age: Implications for the interpretation of chemical weathering rates: Geology, v. 36, p. 35–38, https://doi.org/10.1130/G24285A.1.

Zandt, G., Gilbert, H., Owens, T., Ducea, M., Saleeby, J., and Jones, C.H., 2004, Active foundering of a continental arc root beneath the southern Sierra Nevada in California: Nature, v. 431, p. 41–46, https://doi.org/10.1038/nature02847.